Nature Communications

https://doi.org/10.1038/s41467-026-70678-8

Article in Press

Insights into the activation patterns of 1,2-dithiolane unit in biofunctional molecules

Received: 22 April 2025

Accepted: 3 March 2026

Cite this article as: Zhao, J., Liu, H., Liu, T. *et al.* Insights into the activation patterns of 1,2-dithiolane unit in biofunctional molecules. *Nat Commun* (2026). https://doi.org/10.1038/s41467-026-70678-8

Jintao Zhao, Huimin Liu, Tao Liu, Jun Wu, Bingbing Chang, Tao Ma, Meirong Yi, Shao-Hua Wang, Xinming Li, Baoxin Zhang, Chao Zhang & Jianguo Fang

Insights into the Activation Patterns of 1,2-Dithiolane Unit in Biofunctional Molecules

Jintao Zhao[1, 2, 3, ○], Huimin Liu[4, ○], Tao Liu[2, 3], Jun Wu[2], Bingbing Chang[2], Tao Ma[2], Meirong Yi[2], Shao-Hua Wang[2, 3], Xinming Li[1], Baoxin Zhang[2*], Chao Zhang[4*], and Jianguo Fang[1*]

[1] School of Chemistry and Chemical Engineering, Nanjing University of Science & Technology, Nanjing, Jiangsu 210094, China.

[2] State Key Laboratory of Natural Product Chemistry and College of Chemistry and Chemical Engineering, Lanzhou University, Lanzhou, Gansu 730000, China.

[3] School of Pharmacy, Lanzhou University, Lanzhou, Gansu 730000, China.

[4] Provincial Engineering Laboratory for Screening and Re-evaluation of Active Compounds of Herbal Medicines in Southern Anhui, School of Pharmacy, Wannan Medical College, Wuhu, Anhui 241000, China.

[○] Jintao Zhao and Huimin Liu contributed equally to this study.

[*] Corresponding Authors:

Baoxin Zhang, E-mail: zhangbx@lzu.edu.cn;

Chao Zhang, E-mail: zhangchao@wnmc.edu.cn;

Jianguo Fang, E-mail: fangjg@njust.edu.cn.

Abstract

The cyclic five-membered disulfide 1,2-dithiolane, known for its moderate reactivity and ease of preparation, holds significant promise as a recognition unit in probe design and drug development. However, potential limitations in activation specificity—most notably the diminished selectivity toward thioredoxin reductase (TrxR) caused by nonspecific reactions with abundant low-molecular-weight (LMW) thiols such as glutathione (GSH)—raise concerns about its reliability in biological settings. Here we systematically evaluate the activation behavior of 1,2-dithiolane by synthesizing a panel of prodrugs and fluorescent probes incorporating either amine- or hydroxyl-linked cargoes. Our results reveal that TrxR-mediated selective activation of the 1,2-dithiolane unit is achievable when the cargo is incorporated within an amine-based framework. In contrast, hydroxyl-linked conjugates undergo rapid cleavage by physiological GSH levels, resulting in a pronounced loss of TrxR selectivity. Generally, the recognition site 1,2-dithiolane, the linker unit and the leaving group in a cargo coordinate to determine the selectivity activated by TrxR. Overall, this study resolves ambiguities in previous reports, reconciles conflicting observations, and provides new conceptual guidance for the use of the 1,2-dithiolane scaffold in the design of biofunctional molecules.

1. Introduction

Preservation of redox homeostasis represents an essential biological process governing a myriad of physiological functions.[1, 2, 3, 4] The thioredoxin (Trx) system plays a key role in maintaining cellular redox homeostasis and represents a major thiol-dependent antioxidant system.[5] Within this system, thioredoxin reductase (TrxR) serves as the upstream redox enzyme that couples NADPH-derived reducing power to Trx, thereby enabling dithiol–disulfide exchange reactions in downstream effector proteins.[5, 6] Notably, mammalian TrxRs comprise a unique class of selenoproteins characterized by the presence of a catalytically essential selenocysteine (Sec) residue within their C-terminal redox-active motif. Emerging evidence implicates the dysregulation of TrxR in the pathogenesis of multiple disease states, particularly autoimmune disorders and cancer, positioning this enzymatic system as a highly promising therapeutic target for pharmacological intervention.[6, 7, 8, 9, 10]

Given the essential role of TrxR in biological processes, advancing techniques to monitor and respond to its dynamic behavior is key to deepening our understanding of cellular physiology. Recent advances have yielded diverse activity-based fluorescent probes for TrxR imaging in cells and in vivo.[11, 12, 13, 14, 15, 16, 17, 18, 19, 20] Three principal triggering motifs are incorporated into these molecules: (i) a linear diselenide unit,[16, 19] (ii) a 1,2-thiaselenane ring,[17, 20] and (iii) a 1,2-dithiolane moiety[11, 12, 13, 14, 15, 18] (Fig. 1A). Although linear disulfides are used as TrxR-responsive motifs, in vitro assays conducted under subphysiological GSH concentrations (≤10 μM vs 1–10 mM intracellularly) can obscure TrxR-specific activation by competing thiols, compromising their ability to model native enzyme behavior.[21, 22] We previously developed five 1,2-dithiolane-based fluorescent probes (the TRFS series) for cellular and in vivo imaging, as well as for rapid screening of TrxR inhibitors (Fig. 1B).[11, 12, 13, 14, 15] Furthermore, motivated by the well-documented upregulation of TrxR in tumors,[6, 8, 9] we reported two prodrugs specifically designed to target TrxR for cancer therapy (Fig. 1C).[23, 24] All our molecules are constructed with amine-based cargoes (Fig. 1B, C), displaying favorable selectivity for TrxR (nM concentration) over GSH (mM concentration). Activation paradigms for 1,2-dithiolane-based molecules (e.g., TRFS-green)

involve a TrxR-initiated cascade reaction sequence comprising disulfide reduction, intramolecular cyclization, and cargo release (Fig. 1D).[11] In contrast, the probe Fast-TRFS variant achieves direct fluorescence uncaging through a simplified disulfide cleavage mechanism (Fig. 1E).[15] Some fluorescent probes detect TrxR through covalent binding.[25, 26] However, these compounds substantially inhibit the enzyme, potentially leading to unintended biological consequences.[26, 27] Moreover, considering the low nanomolar abundance of TrxR in cells, covalent probe strategies that rely on stoichiometric enzyme engagement can increase the risk of false-positive or misleading signals. Our evaluations demonstrate a clear correlation between the activation of biomolecular tools based on the 1,2-dithiolane framework and TrxR activity, with cargoes consisting mainly of amine-based drugs or fluorophores. However, recent structural analyses reveal that conjugation of 1,2-dithiolane to a fluorogenic phenolic moiety induces paradoxical activation profiles, wherein promiscuous low-molecular-weight (LMW) thiol-mediated triggering overrides enzymatic specificity.[28] This work calls into question our previous conclusion that TRFS-green is selective for TrxR and concludes based on the probe examined in their study that the apparent non-selective reactivity of 1,2-dithiolane–based molecules stems from the intrinsic chemistry of the ring rather than from variations in the conjugated cargo or linker. To address this inconsistency, we focus on two key mechanistic questions: (i) whether LMW thiols (e.g., GSH) can mediate disulfide bond reduction within 1,2-dithiolane scaffolds, and (ii) the structural determinants governing cargo release versus retention following LMW thiol–mediated cyclic disulfide cleavage. Accordingly, systematic structure–activity relationship (SAR) studies are essential for elucidating the activation thermodynamics and selectivity constraints of 1,2-dithiolane systems bearing distinct cargoes, which support that the recognition site 1,2-dithiolane, the linker unit and the leaving group in a cargo coordinate to determine the selectivity triggered by TrxR (Fig. 2).

In this study, we dissect the SAR underlying cargo-dependent activation of 1,2-dithiolane systems. Using hydroxyl-containing drugs—including (+)-camptothecin (CPT), SN38, gemcitabine (Gem), and paclitaxel (PTX)—we conducted in vitro kinetic assays to assess the reactivity of corresponding prodrugs (S-CPT, S1-SN38, S2-SN38, S1-Gem, S-PTX; Fig. 3) toward

GSH and TrxR. Notably, carbonate (−O−C(O)−O−)-linked conjugates were highly susceptible to non-specific activation by physiological GSH, abolishing TrxR selectivity, highlighting a limitation of linker chemistry rather than the cyclic disulfide trigger. Heterogeneous activation profiles were observed across TrxR-treated prodrugs, exemplified by S-PTX's aberrant stability. We further synthesized prodrugs and probes with amine-containing cargoes (S1-DOX, S2-DOX, S-Cou, S1-Cou; Fig. 3) to examine TrxR selectivity. Our findings demonstrate a clear difference in reactivity between molecules featuring a carbamate (−NH−C(O)−O−) linker and those with a −O−C(O)−O− linker. Cellular evaluation of TRFS-green confirmed its reliability as a TrxR-responsive fluorescent probe, and comparative analysis revealed a clear dichotomy: −NH−C(O)−O− linkers confer TrxR specificity, whereas −O−C(O)−O− linkers lead to promiscuous activation. Taken together, these findings resolve prior inconsistencies in 1,2-dithiolane tools and establish design principles for enhancing TrxR specificity and functionality. Key results are summarized in Fig. 2, with details in the Results section.

2. Results

2.1. Linker- and cargo-dependent design of 1,2-dithiolane prodrugs and probes

In cellular redox environments, reduction-activated "trigger–cargo" systems have been designed to release a variety of cargoes, including fluorophores bearing hydroxyl or amine functionalities, as well as therapeutic compounds.[29, 30, 31, 32, 33, 34, 35, 36, 37, 38, 39] The previously reported TRFS probes employed aniline-based fluorophores as reporter cargoes (Fig. 1B). In prodrug systems, critical functional groups within drug scaffolds are well defined, typically involving a fixed molecular scaffold and a specific chemical bond linking the cargo to the triggering unit. In our earlier investigations of two prodrugs incorporating the 1,2-dithiolane unit, −NH−C(O)−O− linkages were used for conjugation (Fig. 1C). This design choice was dictated by the requirement that the amine functionality remain accessible to ensure intracellular biological activity, despite the presence of additional functional groups within the drug scaffold.[40, 41, 42] Conversely, for drugs where the hydroxyl group serves as the critical active site, using a −O−C(O)−O− linker is essential

to fully explore the properties of 1,2-dithiolane derivatives. However, this strategy was not extensively explored in our prior work. To explore the influence of hydroxyl-based leaving groups in 1,2-dithiolane-based prodrugs, we synthesized five prodrugs—S-CPT, S1-SN38, S2-SN8, S1-Gem, and S-PTX (Fig. 3). Each features a uniform recognition site structure, the 1,2-dithiolane unit, with varying alcohol types as leaving groups: primary (Gem), secondary (PTX), and tertiary (CPT and SN38). The distinction between S1-SN38 and S2-SN38 lies in the specific hydroxyl group protected by the recognition unit: S1-SN38 masks the tertiary hydroxyl group at the C20 position of SN38, whereas S2-SN38 masks the phenolic hydroxyl group at the C10 position. S1-SN38, previously reported by us as a control compound, was re-evaluated in this study.[43] To minimize the risk of false-positive signals arising from thiol-induced attack on −O−C(O)−O− linkers, three corresponding control molecules—C-CPT, C-SN38, and C-PTX—were also synthesized. To further elucidate reactivity differences between amine- and hydroxyl-based prodrug designs, doxorubicin (DOX)-based prodrugs, S1-DOX and S2-DOX, were prepared to assess TrxR selectivity. S1-DOX features a 1,2-dithiolane unit directly conjugated to the aliphatic amine of DOX via a −NH−C(O)−O− linkage. In contrast, S2-DOX incorporates a self-immolative spacer between the recognition unit and DOX, a design commonly employed to facilitate intramolecular reactions, including electron-transfer cascades within aromatic systems.[44, 45] Replacement of sulfur atoms with selenium in S1-DOX and S2-DOX afforded Se1-DOX and Se2-DOX, respectively, enabling further insight into rate-limiting steps in the intramolecular cyclization process. An inactive control compound, C-DOX, corresponding to S1-DOX, was synthesized and employed in cytotoxicity assays. In addition, Se-NBL, a selenium-containing analogue of TRFS-red,[14] was synthesized. Finally, the probes S-Cou and S1-Cou were prepared to evaluate their TrxR selectivity and to determine whether 1,2-dithiolane-based probes derived from aniline exhibit reactivity profiles comparable to those of the TRFS series.

The synthesis of 1,2-dithiolan-4-ol, 1,2-diselenolan-4-ol, and derivative **1** was performed according to our previously reported procedures,[15, 24] whereas intermediates **2** and **3** were prepared via analogous methodologies. Utilizing CPT as the starting material, S-CPT and C-CPT were

synthesized with moderate isolated yields of 40% and 50%, respectively. S1-SN38 was obtained from SN38 through a multistep synthetic sequence involving regioselective functionalization, disulfide coupling, and purification, achieving an overall yield of 22%. S2-SN38 and C-SN38 were generated *via* direct nucleophilic substitution of SN-38 with intermediates **1** and **2**, yielding 20% and 30%, respectively. The preparation of S1-Gem, S-PTX, C-PTX, S1-DOX, S2-DOX, Se1-DOX, Se2-DOX, C-DOX, and Se-NBL followed synthetic routes analogous to S2-SN38, with S1-Gem exhibiting a diminished yield of 8% and other compounds demonstrating yields spanning 10–50%. S-Cou was synthesized using a strategy paralleling the TRFS-green methodology,[11] while S1-Cou was prepared by adapting the Fast-TRFS protocol.[15] Fig. 3 outlines the specific steps, and detailed synthesis procedures and characterization of all final products are provided in the Supplementary Information.

2.2. Hydroxyl cargoes promote GSH-mediated activation of 1,2-dithiolane prodrugs

CPT and its derivative SN38 exhibit intrinsic fluorescence.[36, 46, 47, 48, 49] We observed significant changes in the fluorescence properties of S-CPT, S1-SN38, and S2-SN38 compared to their parent drugs (i.e., CPT and SN38). As shown in Fig. 4A, upon reaction with GSH (1 mM), the fluorescence intensity of S-CPT (10 μM) increased by 4.7-fold within 10 minutes. A comparable outcome was also observed when TrxR (50 nM) was used as the bioactive reducing agent, resulting in a 4.3-fold increase in fluorescence intensity (Fig. 4B). We subsequently conducted fluorescence assays with S1-SN38 (10 μM), which also displayed an "OFF to ON" fluorescence behavior. Upon reaction with GSH (1 mM) or TrxR (50 nM) (Fig. 4C, D), the fluorescence intensity increased by 3.6-fold and 5.2-fold, respectively. Upon incubation with GSH (1 mM) or TrxR (50 nM), the emission wavelength of S2-SN38 (10 μM) shifted from 427 nm to 545 nm within 10 minutes, with a near-complete shift observed (Fig. 4E, F). Collectively, preliminary fluorescence data indicate that the prodrug molecules (i.e., S-CPT, S1-SN38, and S2-SN38) exhibit a lack of TrxR selectivity, regardless of whether the tertiary hydroxyl group from CPT, the hydroxyl group from SN38, or the phenolic hydroxyl group is involved. Fig. 4G illustrates the proposed activation mechanism of

hydroxyl-linked 1,2-dithiolane molecules, exemplified by S-CPT, which was later confirmed by HPLC analyses. Compared to linear disulfide bonds, cyclic disulfide linkages exhibit a more efficient quenching effect on the fluorescence of CPT.[36] This property has important implications for the design of small-molecule fluorescent probes based on cyclic disulfides, as it allows for the development of sensors with improved signal-to-noise ratios.

Prior to evaluating prodrug activation via HPLC, we assessed the stability of the prodrug molecules under test conditions. The results demonstrated that all prodrugs exhibited substantial stability in PBS buffer (pH = 7.4) at 37 ℃ (Supplementary Fig. 1). The stability of 1,2-dithiolane-class prodrugs was further assessed in serum-containing culture medium. All prodrug candidates remained well-stabilized under this condition except for S2–SN38, which exhibited pronounced instability (Supplementary Fig. 2). S2–SN38 underwent rapid degradation in serum-containing medium, with approximately 90% loss within ~20 minutes; this rapid serum-mediated decomposition does not affect the conclusions drawn from experiments conducted in PBS buffer but indicates that S2–SN38 is unsuitable for applications in biological systems. As shown in Fig. 5A–5D, HPLC analysis reveals that, upon reaction with GSH (1 mM), the percentage of cargoes released from S-CPT (10 μM) was 46% within 10 minutes, while S1-SN38 (10 μM) released 17%, S2-SN38 (10 μM) released 90%, S1-Gem (50 μM) released 70%, and S-PTX (20 μM) released 36%. Upon reaction with TrxR (50 nM), the percentage of cargo release was 48% for S-CPT (10 μM), 10% for S1-SN38 (10 μM), 55% for S2-SN38 (10 μM), 34% for S1-Gem (50 μM), and 0% for S-PTX (20 μM). Interestingly, the release kinetics of CPT from its prodrug, S-CPT, upon reaction with GSH, demonstrates that cyclic disulfides act as much more efficient triggering units than linear disulfides. Specifically, when the linear disulfide-based prodrug CPT-S is exposed to 100 equivalents of GSH, it takes over 60 minutes to achieve ~50% of the maximum drug release.[36] In contrast, the corresponding cyclic disulfide prodrug, S-CPT, reaches the same release level in approximately 10 minutes. This striking difference in release dynamics highlights the enhanced efficiency of cyclic disulfides in facilitating rapid prodrug activation. Such an acceleration of drug release could be particularly beneficial for the development of prodrug strategies aimed at

achieving fast, controlled activation in therapeutic applications. The control molecules (i.e., C-CPT, C-SN38, and C-PTX) did not release the parent drugs upon incubation with GSH or TrxR (Supplementary Fig. 4). This observation indicates that the cargo release is attributed to thiol-induced intramolecular cyclization through disulfide bond reduction by GSH or TrxR, rather than a false-positive result due to nucleophilic attack on the −O−C(O)−O− linkage by these reagents. Recent studies employing the –O–C(O)–O– motif for the selective recognition of endogenous redox species, while resisting interference from GSH, lend mechanistic support to the present work.[50, 51] Specifically, GSH-triggered activation of –O–C(O)–O–-based 1,2-dithiolane prodrugs is primarily driven by disulfide bond cleavage and subsequent intramolecular cyclization. Interestingly, GSH (1 mM) can activate S-PTX (20 μM), whereas TrxR (50 nM) cannot. Notably, the comparison between 1 mM GSH and 50 nM TrxR is not intended to imply equivalence, but rather to reflect their physiologically relevant abundance. These conditions were deliberately chosen to recapitulate this intrinsic biological disparity, rather than to achieve stoichiometric comparability.

We then present the residual amounts of various prodrug molecules, which further elucidate their interactions with GSH or TrxR. Mechanistically, the activation of prodrugs involves a cascade reaction, where the interaction with reductants does not necessarily correlate with cargo release. As shown in Fig. 5E–5H, HPLC analysis indicated that, following reaction with GSH (1 mM), the remaining percentages at 10 minutes were 33% for S-CPT (10 μM), 68% for S1-SN38 (10 μM), 0% for S2-SN38 (10 μM), and 0% for S1-Gem (50 μM). Upon reacting with TrxR (50 nM), the remaining percentages for S-CPT (10 μM), S1-SN38 (10 μM), S2-SN38 (10 μM), and S1-Gem (50 μM) were recorded as 40%, 70%, 16%, and 30%, respectively. These results demonstrate that the molecules (i.e., S-CPT, S1-SN38, S2-SN38, and S1-Gem) are capable of responding to both GSH and TrxR; however, an analysis of the cargo release data reveals that the reduction of prodrugs does not fully translate into the corresponding cargoes, as evidenced by the fact that the percentage decrease in prodrugs exceeds the percentage of cargo released. The liquid chromatography PDA absorption peaks of the control compounds C-CPT, C-SN38, and C-PTX

remained unchanged (Supplementary Fig. 4). Additionally, the results demonstrated that GSH (1 mM) rapidly degrades the disulfide bond in S-PTX (20 μM), resulting in 52% of S-PTX (20 μM) remaining after 10 minutes of reaction. In the TrxR (50 nM) reaction system, 99% of S-PTX (20 μM) remained after 10 minutes. Subsequently, the concentrations of each reactant were adjusted to further validate the accuracy of the observed result and the general behavior of S-PTX. Comparable results were obtained: after a 30-minute reaction with GSH (5 mM), S-PTX (10 μM) was nearly fully degraded, whereas in the presence of TrxR (75 nM) for 1 hour, 90% of S-PTX (10 μM) remained intact (Supplementary Fig. 5).

To elucidate the molecular basis of TrxR-mediated activation, we conducted computer-aided docking simulations for four prodrugs—S-CPT, C-CPT, S-PTX, and C-PTX. All compounds yielded favorable docking scores (< −5.0 kcal/mol), suggesting energetically feasible binding interactions (Supplementary Fig. 6). Notably, S-CPT adopted a binding pose positioning its 1,2-dithiolane ring toward the C-terminal Sec residue, with sulfur atoms at 3.6 Å and 3.9 Å from the selenium atom—distances consistent with potential Se–S interactions. In contrast, C-CPT, although its cyclopentane CH_2 carbons were similarly positioned (3.9 Å and 4.5 Å), lacks the reactive disulfide motif and therefore cannot undergo redox activation. Although S-PTX localized near the surface-exposed catalytic site adjacent to the C-terminal Sec residue, its 1,2-dithiolane sulfur atoms were positioned 9.5 Å and 9.8 Å away from the Sec selenium atom—too distant for efficient Se–S interaction—thus explaining its poor TrxR-mediated activation efficiency (for C-PTX, the cyclopentane CH_2 carbons were 7.4 Å and 7.5 Å from Sec). These findings underscore that TrxR-mediated prodrug activation depends not only on binding affinity but also critically on the precise spatial alignment of the reactive disulfide moiety relative to the Sec active site. Collectively, our docking analysis provides mechanistic insight into the differential activation profiles of these prodrugs and emphasizes the dual importance of molecular recognition and geometric complementarity in the rational design of TrxR-selective therapeutics.

2.3. Amino cargoes bias activation toward TrxR in 1,2-dithiolane prodrugs

To clarify the impact of leaving groups in 1,2-dithiolane prodrugs and probes, we evaluated the reactivity of −NH−C(O)−O−-linked molecules carrying amine-based drugs or fluorophores toward LMW thiols and TrxR. Exploiting DOX's intrinsic fluorescence and aliphatic amine, we designed a fluorogenic "trigger-cargo" system using 1,2-dithiolane as the trigger and DOX as the cargo. The fluorescence of DOX is significantly quenched by the incorporated triggering unit (Supplementary Fig. 7). As shown in Fig. 6, S1-DOX (10 μM), S2-DOX (10 μM), Se1-DOX (10 μM), and Se2-DOX (10 μM) all exhibit fluorescence release upon reduction with Dithiothreitol (DTT) (1 mM). The increases in fluorescence were 8.8-fold (12 h), 17-fold (12 h), 7.1-fold (3 h), and 47-fold (5 h), respectively. It is of note that the fluorescence increase is assessed at different time points, reflecting the distinct plateau phases of fluorescence release for each molecule. DTT, a potent disulfide-reducing agent, provides a theoretical maximum for comparison with actual experimental results. In the presence of TrxR (50 nM), the fluorescence enhancements observed for each molecule were as follows: S1-DOX (10 μM), 6.5-fold increase; S2-DOX (10 μM), 4.4-fold increase; Se1-DOX (10 μM), 1.4-fold increase; and Se2-DOX (10 μM), 1.4-fold increase. Following a 24-hour incubation with GSH (5 mM), S1-DOX (10 μM) showed no change, whereas S2-DOX (10 μM) showed an increase of 1.6-fold, Se1-DOX (10 μM) by 1.3-fold, and Se2-DOX (10 μM) by 2.4-fold. Consequently, fluorescence data revealed that both S1-DOX and S2-DOX effectively circumvent GSH-induced interference, even under high GSH conditions (5 mM, corresponding to a prodrug-to-GSH molar ratio of 1:500). The fluorescence release of S1-DOX in the presence of TrxR was comparable to that observed with DTT (8.8-fold for DTT vs. 6.5-fold for TrxR), indicating that DOX can be released through the reducing action of TrxR. While S2-DOX also exhibits enzyme selectivity for TrxR, its release efficiency is markedly lower than that with DTT (17-fold for DTT vs. 4.4-fold for TrxR), emphasizing the differences among various leaving groups. Moreover, both control molecules, Se1-DOX and Se2-DOX, demonstrated resilience against degradation by GSH and TrxR, highlighting the intricate nature of the cascade reaction mechanisms involved. Se-NBL, as a selenium-containing analogue of TRFS-red, exhibits

similar characteristics (Supplementary Fig. 8).[14] Cytotoxicity assays of the DOX-based prodrugs revealed that free DOX exhibited the highest anticancer potency among the three tested tumor cell lines (A549, HeLa, and HepG2). S1-DOX displayed activity ranking second to DOX, while S2-DOX, Se1-DOX, Se2-DOX, and C-DOX showed significantly reduced activity compared to S1-DOX (Supplementary Fig. 9). Remarkably, Se2-DOX exhibited negligible cytotoxicity under all tested conditions, indicating poor activation of the prodrug even within the complex redox microenvironment of living cells. These findings highlight a fundamental limitation of five-membered cyclic diselenide-based delivery systems: despite their higher susceptibility to mild reductive stimuli compared to disulfides, the dominant intramolecular cyclization following bond cleavage markedly hampers efficient cargo release. Notably, the dynamic equilibrium between bond cleavage and molecular reconstitution may also apply to analogous cyclic disulfide systems, offering mechanistic insights that could inform the rational design of next-generation redox-responsive prodrugs and probes.

Building on the observation that S1-DOX exhibits remarkable cytotoxicity in tumor cells and undergoes efficient fluorescence release upon activation by TrxR, we conducted an in-depth investigation into its activation properties. As shown in Fig. 7A, a dose-dependent response to TrxR was observed. S1-DOX (10 μM) exhibited resistance to interference by GSH (5 mM) and did not respond to other LMW thiols, such as cysteine (Cys, 5 mM), or to bioactive substances like NADPH (200 μM) (Fig. 7B, C). HPLC analysis showed that approximately 30% of DOX was released over a 24-hour period in the presence of TrxR (Supplementary Fig. 10). To achieve optimal experimental validation, we implemented CRISPR/Cas9-mediated genome editing to generate a stable TrxR1-knockout (KO) model in human colorectal carcinoma HCT-116 cells.[52] Subsequent western blot analysis demonstrated comparable TrxR1 expression profiles between parental HCT-116 cells and their non-targeting control (NC) counterpart (HCT116-NC), while exhibiting complete absence of TrxR1 protein expression in the engineered HCT116-*TrxR1*-KO clone (Supplementary Fig. 11). Cytotoxicity assays revealed that S1-DOX exerted comparable inhibitory effects across three cell lines (HCT116, HCT116-NC, and HCT116-*TrxR1*-KO), with

IC_{50} values consistently around 0.6 μM (Fig. 7D). This observation indicates that its cytotoxic activity is not solely dependent on TrxR-mediated activation. As noted, carbamate-linked 1,2-dithiolane derivatives can be activated not only by TrxR but also, to a limited extent, by an intact GSH system, as exemplified by TRFS-green.[28] Given the relatively low TrxR-mediated release efficiency of S1-DOX (~30% at 24 h, versus ~80% within 8 h for other 1,2-dithiolane-based prodrugs[23, 24]), even in cells with intact TrxR1, this modest enzymatic activation may still suffice to accumulate cytotoxic levels of the active drug, with additional reduction pathways potentially contributing to overall toxicity. In TrxR1-deficient cells, intrinsic non-TrxR reductive systems, such as the GSH pathway, can be upregulated compensatorily,[53, 54] enhancing S1-DOX reduction. Over prolonged incubation (24 h), these alternative pathways may generate sufficient active compound to induce substantial cytotoxicity. As a result, the TrxR-dependent component of prodrug activation is effectively masked in conventional cytotoxicity assays.

Molecular docking simulations revealed that both S1-DOX and Se1-DOX exhibit favorable binding affinities toward TrxR, with calculated binding energies of −5.981 and −6.007 kcal/mol, respectively (Supplementary Fig. 12). The selenium atom of the Sec residue is positioned 3.7 Å and 4.5 Å from the sulfur atoms of S1-DOX, and 3.8 Å and 4.0 Å from the selenium atoms of Se1-DOX, suggesting spatial proximity conducive to Se–S or Se–Se interactions at the Sec-containing redox center. These results indicate that both prodrugs can stably engage TrxR, enabling potential redox exchange between their disulfide/diselenide motifs and the enzyme's active selenol–thiol pair. However, only S1-DOX undergoes efficient drug release, whereas Se1-DOX remains largely inert. This divergence likely arises from the higher nucleophilicity of the selenol intermediate derived from Se1-DOX, which favors reoxidation to a stable diselenide rather than proceeding through intramolecular cyclization required for payload liberation (as elaborated in the Discussion section).

2.4. Aniline scaffolds dictate structure-dependent TrxR-selective activation of 1,2-dithiolane fluorescent probes

The aniline-based fluorescent probe **S-Cou** was used to evaluate its selectivity toward TrxR. As shown in Fig. 8B–8D, **S-Cou** exhibited a robust 30-fold fluorescence increase after a 60 min reaction with DTT (1 mM). When S-Cou (10 μM) was incubated with TrxR (50 nM) for 3 h, an 18-fold fluorescence enhancement was observed. By contrast, incubation with GSH (5 mM) for 3 h resulted in only a low 4.5-fold increase in fluorescence. This TrxR selectivity is further substantiated by the minimal interference observed from other bioactive molecules. For instance, Cys (5 mM) induced only a modest 3-fold fluorescence increase, while NADPH (200 μM) led to a mere 2-fold enhancement in fluorescence (Supplementary Fig. 13). In addition, we investigated the resistance of TRFS-green to activation by high concentrations of GSH, as prior studies have indicated a 1:100 reaction ratio between TRFS-green and GSH.[11] Our results revealed that when TRFS-green (10 μM) was incubated with TrxR (50 nM) for 3 hours, the fluorescence intensity increased by 7-fold. In contrast, exposure of TRFS-green (10 μM) to GSH (5 mM) under the same conditions led to only a 1.2-fold increase in fluorescence intensity (Supplementary Fig. 14). These observations underscore the pronounced selectivity of TRFS-green for TrxR over GSH. To further explore the properties of a probe incorporating a urea linker analogous to that in Fast-TRFS, we synthesized S1-Cou and assessed its reactivity. Upon exposure to DTT (1 mM), S1-Cou (10 μM) demonstrated a strikingly rapid fluorescence release, exhibiting a 37-fold enhancement within just 5 minutes, indicative of an efficient and fast-acting disulfide cleavage mechanism (Fig. 8F). In stark contrast, when S1-Cou (10 μM) was incubated with either TrxR (50 nM) or GSH (5 mM), the fluorescence response was minimal, showing only a 2.1-fold increase with TrxR and no detectable change with GSH (Fig. 8G, H). This stark difference suggests that the disulfide bond in S1-Cou remains highly resistant to reduction by these bioactive cellular reducing agents. Notably, the serendipitous discovery of Fast-TRFS catalyzed our ongoing efforts to design long-wavelength (> 600 nm) probes operating via similar fluorescence mechanisms for TrxR detection. However, despite significant effort, extending this mechanism to longer-wavelength emitting probes has proved challenging, and achieving this goal remains elusive.

2.5. TrxR drives fluorescence release of structurally distinct S-Cou and TRFS-green in cells

We next assessed the specificity of two 1,2-dithiolane-based fluorescent probes, S-Cou and TRFS-green, for TrxR activation in cellular environments. Of note, the TrxR-selective fluorescence imaging capacity of TRFS-green has been questioned,[28] prompting a comprehensive re-evaluation of its cellular behavior in this study. As depicted in Fig. 9A, the fluorescence signal of S-Cou remained exceptionally weak after 4 hours of probe incubation, attributed to the misalignment between the fluorescence emission wavelength of S-Cou and the detection range of the confocal microscope. To corroborate these findings, we conducted parallel validation studies employing another fluorescence microscopy in conjunction with AFC-SS—a structurally analogous, well-characterized thiol-activated probe.[55] Fluorescence image analysis revealed robust intracellular fluorescence generation by S-Cou (Supplementary Fig. 15), confirming its metabolic activation capability. Flow cytometric analysis indicated an approximately 30% decrease in S-Cou fluorescence intensity in HCT116-*TrxR1*-KO cells compared with HCT116-NC cells (Fig. 9B; Supplementary Fig. 16), indicating that the intracellular activation of S-Cou is closely associated with TrxR activity. Confocal microscopy showed marked attenuation of TRFS-green fluorescence in HCT116-*TrxR1*-KO cells (Fig. 9C), with flow cytometric analysis quantifying an approximately 80% diminution in signal intensity relative to HCT116-NC cells (Fig. 9D). To rigorously establish TrxR selectivity of TRFS-green, we employed TRi-1—a highly selective TrxR1 inhibitor.[56] Dose-response studies showed concentration-dependent suppression of TRFS-green fluorescence (Fig. 9E, F), with 2 μM TRi-1 producing an approximately 30% reduction in signal intensity. By comparison, the same concentration of the reference TrxR inhibitor auranofin (AF) resulted in an approximately 45% decrease in fluorescence (Fig. 9F). A representative gating strategy used for all flow cytometry experiments in this study is shown in Supplementary Fig. 17. The concentration of TRi-1 was selected based on its inhibitory effect on TrxR activity in HCT116 cells (Supplementary Fig. 18).

Therefore, these systematic variations in chemical and biological reductants, along with comprehensive time-course and endpoint analyses, highlight a crucial observation: under our experimental conditions, 1,2-dithiolane-based prodrugs and probes—particularly those with amine-based drugs or fluorophores as cargoes—demonstrate a distinct selectivity for TrxR. Even at elevated concentrations (i.e., 5 mM), LMW thiols (e.g., GSH and Cys) did not activate these biofunctional agents. Cellular fluorescence imaging and flow cytometric analysis further strengthen the foundation of our conclusions.

3. Discussion

3.1. Avoiding nonspecific activation via 1,2-dithiolane-based design

Quantifying the activity of key cellular redox regulators, particularly oxidoreductases such as TrxR, is essential for understanding physiological redox homeostasis and for targeting dysregulated redox states in pathological conditions.[24, 30, 57, 58, 59, 60, 61, 62] Linear disulfides have been widely employed as redox-responsive triggering groups. These triggers are prone to non-specific activation by LMW thiols, such as GSH, as well as by thiol-containing proteins, severely limiting their utility in biological applications, particularly in vivo.[24, 59, 63, 64] Although previous studies, including our own, have reported linear disulfide-based sensors capable of bypassing GSH interference under specific experimental conditions, it is now clear that over extended timescales and within the more complex intracellular redox milieu, these molecules fail to maintain selectivity for a defined redox species.[21, 22, 61, 65, 66, 67] Therefore, achieving selectivity toward a specific redox enzyme requires overcoming two key challenges: (1) avoiding interference from thiol-rich cellular proteins, and (2) preventing activation by high intracellular LMW thiols. In response to these challenges, our group has developed a series of 1,2-dithiolane-based fluorescent probes and prodrugs, which are selectively activated by TrxR, as supported by comprehensive experimental evidence. Notably, these 1,2-dithiolane scaffolds exhibit high resistance to GSH-mediated activation, and exemplars such as S1-Puro demonstrate exceptional stability in human plasma ($t_{1/2}$ > 48 h).[24] Collectively, 1,2-dithiolane-based molecular designs effectively overcome the limitations

of linear disulfides, providing a robust and selective platform for redox-targeted chemical biology and therapeutic applications.

3.2. Enabling TrxR-selective activation through amine-directed 1,2-dithiolanes

A recent report has raised questions about our previous work,[28] an inquiry we both welcome and encourage, as such challenges contribute significantly to a deeper understanding of the field. Although the data and methodologies presented in the report are thorough, we offer a different interpretation of their conclusions. Specifically, (1) In their study, the authors reported that the 1,2-dithiolane-based probe SS50-PQ demonstrated non-selective reductive activation, with the key observation being its rapid and efficient response to LMW thiols. They inferred that 1,2-dithiolane-based probes, such as SS50-PQ and TRFS probes, are intrinsically unable to selectively report on TrxR activity. The conclusion attributes this lack of selectivity to the inherent properties of the 1,2-dithiolane scaffold, suggesting that this behavior is independent of the appended cargo or the nature of its chemical linkage. However, we take a different scientific stance. we propose that the TrxR selectivity of 1,2-dithiolane-based probes is largely determined by the molecular components surrounding the disulifide-based trigger, particularly the leaving group and the linker. Accordingly, we designed five 1,2-dithiolane-based prodrugs (i.e., S-CPT, S1-SN38, S2-SN38, S1-Gem, and S-PTX) with hydroxyl-based drugs as leaving groups. Our findings reveal that these prodrug molecules, featuring primary, secondary, and tertiary alcohols, as well as phenolic hydroxyls as leaving groups, are broadly susceptible to activation by a range of cellular reductants, including GSH and TrxR. However, the 1,2-dithiolane molecules incorporating amino groups (i.e., S-Cou and S1-DOX) remain consistent with our previously reported findings, aligning with the behavior of TRFS probes and the prodrugs S-Gem and S1-Puro.[12, 13, 14, 15, 23, 24] Notably, certain amino group-loaded 1,2-dithiolane derivatives can effectively minimize interference from LMW thiols, the intricate cellular environment presents more stringent challenges. For example, while S-Cou signal activation in cells is closely linked to TrxR activity, its TrxR dependence is less pronounced than that of TRFS-green. S1-DOX, though TrxR-selective in cell-free assays, is still activated by other

intracellular reductants, masking its TrxR-specific cytotoxicity. (2) The report also questioned whether TRFS-green is exclusively activated by the TrxR, as their findings suggest that other intracellular proteins, such as Glutaredoxin (Grx), are also capable of activating this probe. Another study from our collaborators and us demonstrated the utility of TRFS-green in detecting the overall disulfide reduction activity in bacterial cells.[68] TRFS-green was also identified as a substrate for the complete bacterial Trx system (TrxR/Trx/NADPH) and the GSH system (Glutathione Reductase (GR), GSH, NADPH, and Grx), but it was not activated by GSH, GR, or bacterial TrxR alone. While both complete redox systems are capable of activating TRFS-green, the Trx system produces significantly stronger fluorescence. Fast-TRFS exhibited a comparable activation pattern.[69] These findings does not contradict our previous results, as bacterial TrxR contains only a single N-terminal active site, while mammalian TrxRs have a C-terminal active site with a characteristic GCUG motif. This structural distinction suggests that the C-terminal site plays a crucial role in activating TRFS probes (e.g., TRFS-green and Fast-TRFS) in mammalian TrxRs. In Accordingly, integrating our results with prior reports and established biochemical principles, the evidence indicates that additional intracellular species must contribute to the activation of TRFS probes. Nonetheless, TRFS probes provide a reliable and practical readout of TrxR activity in the complex cellular environment. Recent studies utilizing TrxR-overexpressing and knockout cell lines have further demonstrated the predominant role of TrxR in mediating the TRFS-green signal, reinforcing the notion that, despite the potential contributions from other bioactive species, TrxR plays the central role.[52, 70] To date, TRFS-green has been successfully commercialized and is now used by researchers in various scientific investigations.[71, 72, 73, 74, 75, 76, 77, 78, 79, 80, 81, 82, 83]

In this work, we rigorously reassessed TRFS-green's cellular responsiveness to TrxR through TrxR1 knockout and chemical inhibition experiments. The results collectively confirm the reliability of TRFS-green as a high-selectivity probe for TrxR. Notably, although TRFS-green exhibits detectable responses beyond TrxR in cell-free assays,[28] its fluorescence is markedly diminished in TrxR1-knockout HCT116 cells. This can be explained by its activation hierarchy: in

intact redox systems, TRFS-green is rapidly and efficiently reduced by TrxR in the presence of NADPH, a process further accelerated by Trx. In contrast, activation via the GSH system requires the full enzymatic network (GSH, GR, Grx, and NADPH) and, even under optimal conditions, produces a significantly weaker signal compared to TrxR-mediated reduction.[28, 68] Although the loss of TrxR may induce compensatory upregulation of the GSH pathway, its contribution to probe activation is likely minimal during short incubation periods (typically ≤ 4 h). Collectively, these factors provide a coherent explanation for the substantially reduced fluorescence observed in TrxR-deficient cells.

3.3. Tuning 1,2-dithiolane reactivity for orthogonal activation pathways

A critical structure–reactivity paradox arises from these findings: which molecular features govern the distinct bioactivation patterns of 1,2-dithiolane-containing molecules, particularly their differential activation via GSH-dependent pathways? Deciphering this SAR requires a systematic interrogation of two sequential biochemical events: (i) the reductive lability of the dithiolane scaffold in intracellular redox environments and (ii) the chemical trajectory of nascent thiol species—specifically, their propensity for intramolecular cyclization-mediated cargo release versus thiol-disulfide exchange reactions. The reduction and cleavage of 1,2-dithiolane by GSH is a widely observed phenomenon in nature, exemplified by lipoic acid—a natural product bearing a 1,2-dithiolane scaffold that serves as an important cofactor in cellular redox processes. Extensive studies have revealed that lipoic acid plays a pivotal role in maintaining redox homeostasis, it lacks selectivity for specific redox species.[84, 85, 86] In previous investigations into the properties of various 1,2-dithiolane derivatives, we explored the reduction kinetics of five- and six-membered cyclic disulfides and diselenides by the TrxR and GR systems, observing that while both systems efficiently reduced these substrates, their reduction rates diverged significantly for particular compounds.[15] Studies have shown that the Trx system can exhibit superior catalytic efficiency over the GSH system in reducing disulfides of various configurations, including both linear and cyclic forms.[15, 65, 87, 88] Mechanistic investigations demonstrated that when the 1,2-dithiolane

moiety was conjugated via carbamate linkages to targeted molecular architectures for the development of stimuli-responsive prodrugs or probes, GSH mediated only partial reduction of the intracyclic disulfide bonds, whereas TrxR consistently exhibited markedly higher catalytic efficiency in the cleavage process.[23, 24]

As delineated in Fig. 10A, we postulate an enzymatic reduction mechanism wherein molecule **a** undergoes TrxR-mediated reduction to generate intermediate **b**, followed by its stereoelectronic optimization-driven conversion to **c** through a preorganized unimolecular transition state that exploits TrxR's catalytic architecture.[17] Contrastingly, GSH-mediated reduction of **a** produces intermediate **d**, which undergoes reversion to **a** via pathway **e**—a process governed by the exceptional kinetic stability of the carbamate linkage. This regioselective thiol-disulfide exchange over carbamate carbonyl attack arises from the suppressed dissociation propensity of the amino-based cargo, thereby establishing a thermodynamically favored pathway.[17, 89, 90] This mechanistic framework rationalizes the observed GSH resistance in 1,2-dithiolanes bearing amine conjugates. Notably, the GSH-mediated disulfide reduction kinetics of **a** exhibit significantly slower rates compared to TrxR-catalyzed processes, rendering the probability of GSH-driven progression to **c** statistically negligible and consequently yielding suboptimal cargo release efficiency. [23, 24] However, strategic substitution of the leaving group with hydroxyl functionality induces a paradigm shift in GSH responsiveness (Fig. 10B). In this modified system, GSH reduction of molecule **f** initiates disulfide cleavage, with the liberated thiol undergoing carbonate bond lability-driven structural reorganization via pathway **g** to achieve cargo liberation. The competing pathway **h** represents a non-productive thiol recycling mechanism. Molecule **f** undergoes a reaction with TrxR through a pathway similar to that of molecule **a**. Collectively, our findings establish the 1,2-dithiolane architecture as a dual-mode molecular scaffold—through strategic incorporation of hydroxyl or amino moieties as cargoes—that achieves orthogonal responsiveness to distinct redox regulators (e.g., thiols vs. TrxR) (Fig. 10C). This modular design paradigm enables programmable activation specificity, thereby establishing a versatile platform for developing precision redox-responsive tools in targeted therapeutics and mechanistic biology.

3.4. Moving beyond trigger-centric reductionism with integrated molecular design

Notwithstanding theoretical reaction paradigms, the operational complexity of enzyme-substrate interplay in biological matrices resists reductionist mechanistic interpretation. A case in point is the dichotomous behavior observed with prodrug S-PTX: while undergoing rapid GSH-dependent bioactivation through thiol-disulfide exchange, the molecule demonstrates complete refractoriness to TrxR-mediated cargo release. We posit this selectivity stems from steric incompatibility between TrxR's catalytic architecture and the spatial orientation of S-PTX's dithiolane moiety, effectively precluding productive engagement with the enzyme's redox-active C-terminal Sec residue. This hypothesis is supported by the results of molecular docking simulations. Furthermore, S1-Cou remains completely inert to both TrxR and GSH, despite its close structural resemblance to Fast-TRFS, suggesting that neither system is capable of cleaving the disulfide bond within S1-Cou. This contrast underscores the critical limitation in extrapolating reactivity patterns across 1,2-dithiolane derivatives—each congener demands rigorous empirical interrogation of its unique SAR through orthogonal analytical methodologies. Our findings necessitate a paradigm of chemical skepticism: the biological trajectory of redox-responsive molecular tools proves exquisitely sensitive to subtle stereoelectronic perturbations. We therefore advocate for systematic deconstruction of structure-function correlations through iterative design-test cycles, cautioning against mechanistic generalizations until comprehensive validation across multiple biological contexts is achieved.

3.5. Prioritizing adaptive probe performance over static specificity metrics

Small-molecule probes, ligands, and inhibitors inevitably experience off-target interactions—particularly in redox-active systems where enzymes such as TrxR, GR, and other oxidoreductases share overlapping catalytic motifs, cofactors, and substrate preferences. This intrinsic biochemical promiscuity is further amplified by the spatiotemporal heterogeneity of intracellular environments: local reductant concentrations, subcellular compartmentalization, and dynamic protein–protein

interactions can all significantly reshape a probe's activation profile. As recently reported by Thorn-Seshold et al., a 1,2-thiaselenane-based probe originally developed for selective TrxR detection was readily activated by the complete GSH system in cell-free assays and cellular studies further confirmed that TrxR is not its sole activating species.[20] Such findings underscore a central challenge in chemical biology: within highly interconnected and partially redundant redox networks, achieving absolute molecular selectivity is inherently difficult—if not fundamentally unrealistic. Accordingly, probes should not be expected to exhibit absolute exclusivity toward a single molecular target under all circumstances. Instead, the more meaningful design goal is to achieve functional selectivity—the ability of a probe to preferentially and reproducibly report the activity of the intended target under physiologically relevant conditions, even when competing pathways are present. When probe-based readouts are integrated with orthogonal biochemical assays, genetic perturbation studies (e.g., knockout or overexpression), and complementary omics or imaging data, they become powerful tools not only for target detection but also for dynamic interrogation of network behavior and redox regulation. Shifting the design and validation paradigm from unattainable absolute specificity toward context-dependent functional selectivity therefore provides a more realistic, informative, and scientifically productive framework for both probe development and biological interpretation.

3.6. Overcoming limitations through complementary molecular recognition strategies

This study underscores the essential role of incorporating an amine-based structural framework within five-membered cyclic disulfide (i.e., 1,2-dithiolan-4-ol) biofunctional architectures to achieve selective TrxR activation. However, the broader implementation of this methodology is fundamentally limited by the absence of inherent amine functionalities in numerous therapeutic agents and fluorophores. To address this substrate compatibility challenge, we systematically explored aminobenzyl alcohol as a versatile molecular template for expanding the TrxR-activatable chemical space. Unfortunately, the practical implementation of this approach proved challenging, as exemplified by the suboptimal cargo release efficiency observed in template-

derived constructs (e.g., S2-DOX). Notably, recent advances documented in the literature have demonstrated the efficacy of 1,2-thiaselenane motif as alternative TrxR recognition elements, employing hydroxyl-group integration as a key design principle.[17] We propose that these orthogonal strategies—amine-centric molecular engineering versus hydroxyl-mediated recognition—exhibit complementary mechanistic advantages. Rather than representing competing paradigms, their synergistic integration establishes a multi-faceted platform for rational design of precision biomolecular tools. This dual-approach framework significantly enhances our capacity to engineer target-specific functional molecules for TrxR, potentially overcoming current limitations in selectivity and activation efficiency.

In summary, this study reveals that selective targeting of TrxR by 1,2-dithiolane-based biofunctional molecules necessitates the incorporation of an −NH−C(O)−O− linker to connect the amino group to the recognition site. Furthermore, variations in the structure of the amino cargoes result in distinct selectivity profiles for TrxR. Notably, when the hydroxyl group serves as a leaving group, GSH facilitates the rapid activation of these molecules. These findings offer key insights into reconciling discrepancies in the existing literature on 1,2-dithiolane-based prodrugs and probes. By elucidating these mechanistic intricacies, this study advances our understanding of 1,2-dithiolane-based tools and paves the way for developing more precise probes, thereby enhancing their specificity and applicability in complex biological systems.

4. Methods

4.1. Chemical synthesis and drug release

Full details of chemical synthesis, drug release experiments, and compound characterization are described in the Supplementary Information.

4.2. Materials and instrumentations

All chemicals and reagents were used as received from commercial suppliers unless otherwise specified. Solvents were purified and dried using standard procedures prior to use. DMSO, Dulbecco's modified Eagle's medium (DMEM), GSH, NADPH, Cys, DTT, and GSSG were purchased from Sigma-Aldrich (St. Louis, USA). 3-(4,5-Dimethylthiazol-2-yl)-2,5-diphenyltetrazolium bromide (MTT), penicillin, and streptomycin were obtained from Sangon (Shanghai, China). TRi-1 was synthesized according to the method described in the published study.[56] Two independent batches of recombinant rat TrxR1 were used in this study. The first batch was kindly provided by Dr. Jianqiang Xu (Dalian University of Technology, China), and the second batch was provided by Prof. Chao Zhang (Wannan Medical College, China). The following antibodies were used: TrxR1 antibody (Abcam, catalog no. ab124954, dilution 1:2000) and GAPDH antibody (Abcam, catalog no. ab8245, dilution 1:5000).

Mass spectrometry (MS) was performed on a Bruker Daltonics Esquire 6000 or a Shimadzu LCMS-2020 mass spectrometer. Flow cytometry was performed using an ACEA Biosciences NovoCyte flow cytometer and a BD FACSVerse flow cytometer. Confocal fluorescence imaging was carried out on a Leica SP8 confocal microscope. HPLC analyses were conducted using a Shimadzu system equipped with an SPD-M20A photodiode array detector. Fluorescence spectroscopy measurements were carried out using a Thermo Scientific Lumina fluorescence spectrometer. The acquired fluorescence spectra were analyzed using Thermo Scientific Lumina software (version 4.3, build 1). Microplate-based assays were conducted on a BioTek Cytation 5 multimode microplate reader.

4.3. Cell viability assay

The cytotoxicity of DOX HCl, S1-DOX, S2-DOX, Se1-DOX, Se2-DOX, and C-DOX was assessed in A549, HepG2, and HeLa cells using the MTT assay. For this, 8×10^3 cells were seeded into 96-well plates and incubated for 12 hours to allow attachment. The cells were then treated with varying concentrations of the prodrugs for 48 hours. Following treatment, the medium was discarded, and 100 μL of fresh medium containing MTT (0.5 mg mL^{-1}) was added to each well and incubated for an additional 4 hours at 37 °C. Subsequently, 100 μL of extraction buffer (10% SDS, 5% isobutanol, and 0.1% HCl) was added to each well, and the cells were further incubated for 8 hours at 37°C. The absorbance was measured at 570 nm using a microplate reader.

The cytotoxicity of S1-DOX was evaluated in HCT116, HCT116-NC, and HCT116-*TrxR1*-KO cells using the CCK-8 assay. Briefly, 5000 cells per well were seeded in 96-well plates and allowed to adhere overnight. The cells were then treated with serial dilutions of S1-DOX (eight concentrations, starting from 20 μM with a fourfold dilution factor). Blank wells received complete medium without drug, while control wells were treated with an equivalent volume of DMSO. After 24 h of incubation, 10 μL of CCK-8 reagent was added to each well and the plates were further incubated at 37 °C for 2 h. The absorbance at 450 nm was measured using a Cytation 5 microplate reader (BioTek). The cell growth inhibition rate was calculated according to the formula: Growth inhibition rate = (AB value of control - AB value of test) / (AB value of control - AB value of blank) × 100%.

4.4. Cell lines and culture conditions

HeLa, HepG2, A549, and HCT116 cell lines were obtained from the Shanghai Institute of Biochemistry and Cell Biology, Chinese Academy of Sciences (HeLa, SCSP-504; HepG2, SCSP-510; A549, SCSP-503; HCT116, SCSP-5076). HeLa, HepG2, and A549 cells were cultured in DMEM supplemented with 10% fetal bovine serum (FBS), 2 mM glutamine, and 100 U mL^{-1} penicillin–streptomycin, and maintained at 37 °C in a humidified atmosphere containing 5% CO_2. HCT116, HCT116-NC, and HCT116-*TrxR1*-KO cells were cultured in RPMI-1640 medium. The HCT116-NC and HCT116-*TrxR1*-KO cell lines were generated by Prof. Chao Zhang.[52]

HeLa, HepG2, A549 and HCT116 cell lines were authenticated by STR profiling prior to use. HCT116-NC and HCT116-*TrxR1*-KO cell lines were generated by genetic editing based on the parental HCT116 cell line. The identity of these derived cell lines was verified by confirmation of their parental origin and by validation of the intended genetic modifications, rather than by independent STR profiling.

4.5. Live cell imaging and flow cytometry-based fluorescence quantification assay

For both TRFS-green and S-Cou, HCT116, HCT116-NC, and HCT116-*TrxR1*-KO cells were treated with the specified concentrations (10 μM) of probes for the indicated time periods (4 h). Fluorescence images were captured using a Leica SP8 laser scanning confocal microscope. For TRFS-green, fluorescence intensity in each group was quantified using a Novocyte flow cytometer with NovoExpress 1.2.4 software. For S-Cou, fluorescence intensity in each group was measured using a BD FACSVerse flow cytometer (San Diego, CA, USA) with FlowJo 10.9 software. In the TRi-1 inhibition assay, HCT116 cells were treated with the specified concentrations of TRi-1 (negative control: equivalent volume of DMSO; positive control: auranofin (AF)) for 4 hours, followed by an additional 4-hour incubation with TRFS-green (10 μM). Fluorescence images were obtained using the Leica SP8 laser scanning confocal microscope, and the fluorescence intensity in each group was quantified using the Novocyte flow cytometer with NovoExpress 1.2.4 software.

4.6. Assessment of TrxR1 enzyme activity in TrxR1-KO and TRi-1 inhibitor-mediated suppression of cellular TrxR1 activity

For the assessment of TrxR1 cellular enzyme activity, cells were seeded in cell culture dishes. Once cell confluence reached over 90%, the cells were trypsinized, centrifuged, and collected. Proteins were then extracted and quantified using the BCA method. TrxR1 activity in the aforementioned cells was measured using an insulin endpoint enzyme activity assay. A total of 20 μg of cellular protein was incubated with 50 μL of a buffer containing 100 mM Tris-HCl (pH 7.6), 0.3 mM insulin, 660 μM NADPH, 3 mM EDTA, and 1.3 μM Trx protein at 37°C for 1 hour. The reaction was terminated by adding 200 μL of 6 M guanidine hydrochloride containing 1 mM DTNB (pH 8.0). Absorbance (AB) was measured at 412 nm using a Cytation 5 microplate reader

(BioTek). A standard curve was generated using rat liver TrxR1 protein (218.53 U/mg, Sigma), diluted across a series of concentrations, and the TrxR1 enzyme activity in each sample was calculated based on this standard curve.

For the TRi-1 inhibition assay, cells were treated with TRi-1 for 4 hours (starting at 10 μM, with 2-fold dilutions for 6 concentrations). Total cellular protein extraction and TrxR1 activity assays were performed as described above. The same amounts of DMSO were added to the control experiments, and the TrxR1 inhibitory rate was calculated using the following formula: TrxR1 inhibitory rate = [1 - (AB value of sample - AB value of $blank_{sample}$) / (AB value of control - AB value of $blank_{control}$)] × 100%.

4.7. Molecular docking simulation

Molecular docking simulations were conducted using AutoDock Vina (v1.1.2) to predict the binding modes and affinities of the compounds toward TrxR1 (PDB ID: 3QFA). The protein structure was prepared by removing water molecules and co-crystallized ligands, followed by the addition of polar hydrogens and Kollman charges using AutoDock Tools (v1.5.7).[91, 92] The lowest-energy docking pose for each ligand was selected for visualization and analysis in PyMOL (v3.1.6.1), with particular attention to measuring the distance between the ligand's disulfide ring and the selenium atom of Sec498 to validate the binding geometry.

4.8. Statistics analysis

Statistical analyses were performed using Origin 2019 (OriginLab). Data are presented as mean ± SD. Comparisons among multiple groups were conducted using one-way ANOVA. A P value of less than 0.05 was considered statistically significant.

5. Data availability

The data supporting the findings of this study are available in the main text and Supplementary Information, and from the corresponding author(s) upon request. Source data are provided with this paper.

6. References

1. Sies H, Mailloux RJ, Jakob U. Fundamentals of redox regulation in biology. *Nat Rev Mol Cell Bio* **25**, 701-719 (2024).

2. Lennicke C, Cochemé HMJMC. Redox metabolism: ROS as specific molecular regulators of cell signaling and function. *Mol Cell* **81**, 3691-3707 (2021).

3. D'Autréaux B, Toledano MB. ROS as signalling molecules: mechanisms that generate specificity in ROS homeostasis. *Nat Rev Mol Cell Bio* **8**, 813-824 (2007).

4. Shadel GS, Horvath TL. Mitochondrial ROS signaling in organismal homeostasis. *Cell* **163**, 560-569 (2015).

5. Arnér ES, Holmgren AJEjob. Physiological functions of thioredoxin and thioredoxin reductase. *Eur J Biochem* **267**, 6102-6109 (2000).

6. Zhang J, Li X, Han X, Liu R, Fang J. Targeting the thioredoxin system for cancer therapy. *Trends Pharmacol Sci* **38**, 794-808 (2017).

7. Turanov AA*, et al.* Mammalian thioredoxin reductase 1: roles in redox homoeostasis and characterization of cellular targets. *Biochem J* **430**, 285-293 (2010).

8. Ardini M*, et al.* The "Doorstop Pocket" in thioredoxin reductases─an unexpected druggable regulator of the catalytic machinery. *J Med Chem* **67**, 15947-15967 (2024).

9. Gencheva R, Arnér ESJ. Thioredoxin reductase inhibition for cancer therapy. *Annu Rev Pharmacol* **62**, 177-196 (2022).

10. Wientjens C*, et al.* Tolerance to ferroptosis facilitates lipid metabolism and pathogenic type 2 immunity in allergic airway inflammation. *Immunity* **59**, 1-17 (2025).

11. Zhang L*, et al.* Highly selective off–on fluorescent probe for imaging thioredoxin reductase in living cells. *J Am Chem Soc* **136**, 226-233 (2014).

12. Liu Y, Ma H, Zhang L, Cui Y, Liu X, Fang J. A small molecule probe reveals declined mitochondrial thioredoxin reductase activity in a Parkinson's disease model. *Chem Commun* **52**, 2296-2299 (2016).

13. Zhao J*, et al.* Loss of thioredoxin reductase function in a mouse stroke model disclosed by a two-photon fluorescent probe. *Chem Commun* **56**, 14075-14078 (2020).

14. Ma H, Zhang J, Zhang Z, Liu Y, Fang J. A fast response and red emission probe for mammalian thioredoxin reductase. *Chem Commun* **52**, 12060-12063 (2016).

15. Li X*, et al.* A fast and specific fluorescent probe for thioredoxin reductase that works via disulphide bond cleavage. *Nat Commun* **10**, 2745 (2019).

16. Mafireyi TJ, Laws M, Bassett JW, Cassidy PB, Escobedo JO, Strongin RM. A diselenide turn-on fluorescent probe for the detection of thioredoxin reductase. *Angew Chem, Int Ed* **59**, 15147-15151 (2020).

17. Zeisel L*, et al.* Selective cellular probes for mammalian thioredoxin reductase TrxR1: Rational design of RX1, a modular 1,2-thiaselenane redox probe. *Chem* **8**, 1493-1517 (2022).

18. Yang Y-P*, et al.* Fast imaging of mitochondrial thioredoxin reductase using a styrylpyridinium-based two-photon

ratiometric fluorescent probe. *Anal Chem* **94**, 4970-4978 (2022).

19. Zhang Q*, et al.* CBNP: An anti-photobleaching probe for detecting thioredoxin reductase activity in cancer cells. *Microchem J* **219**, 115906 (2025).

20. Mauker P*, et al.* A modular scaffold for cellularly-retained fluorogenic probes for sensitive cell-resolved bioactivity imaging. *Chem Sci* **16**, 22630–22637 (2025).

21. Sidhu JS, Singh A, Garg N, Singh N. Carbon dot based, naphthalimide coupled FRET pair for highly selective ratiometric detection of thioredoxin reductase and cancer screening. *ACS Applied Materials & Interfaces* **9**, 25847-25856 (2017).

22. Yan F*, et al.* High-throughput fluorescent screening of thioredoxin reductase inhibitors to inhibit Mycobacterium tuberculosis. *Chinese Chem Lett* **35**, 108504 (2024).

23. Li X*, et al.* Selective activation of a prodrug by thioredoxin reductase providing a strategy to target cancer cells. *Angew Chem, Int Ed* **57**, 6141-6145 (2018).

24. Chang B*, et al.* Puromycin prodrug activation by thioredoxin reductase overcomes its promiscuous cytotoxicity. *J Med Chem* **66**, 3250-3261 (2023).

25. Huang L*, et al.* A furanyl acryl conjugated coumarin as an efficient inhibitor and a highly selective off-on fluorescent probe for covalent labelling of thioredoxin reductase. *Chem Commun* **50**, 6987-6990 (2014).

26. Liang B*, et al.* Mitochondria-targeted approach: remarkably enhanced cellular bioactivities of TPP2a as selective inhibitor and probe toward TrxR. *Acs Chem Biol* **11**, 425-434 (2016).

27. Zhang J, Zhang B, Li X, Han X, Liu R, Fang J. Small molecule inhibitors of mammalian thioredoxin reductase as potential anticancer agents: an update. *Med Res Rev* **39**, 5-39 (2019).

28. Felber JG*, et al.* Cyclic 5-membered disulfides are not selective substrates of thioredoxin reductase, but are opened nonspecifically. *Nat Commun* **13**, 1754 (2022).

29. Lee MH, Sessler JL, Kim JS. Disulfide-based multifunctional conjugates for targeted theranostic drug delivery. *Acc Chem Res* **48**, 2935-2946 (2015).

30. Lee MH*, et al.* Disulfide-cleavage-triggered chemosensors and their biological applications. *Chem Rev* **113**, 5071-5109 (2013).

31. Wang P, Gong Q, Hu J, Li X, Zhang X. Reactive oxygen species (ROS)-responsive prodrugs, probes, and theranostic prodrugs: applications in the ROS-related diseases. *J Med Chem* **64**, 298-325 (2021).

32. Wang H, Monroe M, Leslie F, Flexner C, Cui H. Supramolecular nanomedicines through rational design of self-assembling prodrugs. *Trends Pharmacol Sci* **43**, 510-521 (2022).

33. Shin WS, Han J, Verwilst P, Kumar R, Kim JH, Kim JS. Cancer targeted enzymatic theranostic prodrug: precise diagnosis and chemotherapy. *Bioconjugate Chem* **27**, 1419-1426 (2016).

34. Liu W*, et al.* Hypoxia-activated anticancer prodrug for bioimaging, tracking drug release, and anticancer application. *Bioconjugate Chem* **29**, 3332-3343 (2018).

35. Kumar R*, et al.* Hypoxia-directed and activated theranostic agent: imaging and treatment of solid tumor. *Biomaterials* **104**, 119-128 (2016).

36. Zhao J*, et al.* Integration of a diselenide unit generates fluorogenic camptothecin prodrugs with improved cytotoxicity to cancer cells. *J Med Chem* **64**, 17979-17991 (2021).

37. Yang Y*, et al.* Thiol–chromene "Click" reaction triggered self-Immolative for NIR visualization of thiol flux in physiology and pathology of living cells and mice. *J Am Chem Soc* **142**, 1614-1620 (2020).

38. Hu G, Xu H-d, Fang J. Sulfur-based fluorescent probes for biological analysis: a review. *Talanta* **279**, 126515 (2024).

39. Ma T*, et al.* Selenenylsulfide bond as a general scaffold for constructing thiol probes with enhanced response rate. *Anal Chem* **97**, 6629-6637 (2025).

40. Ciccolini J, Mercier C, Dahan L, André N. Integrating pharmacogenetics into gemcitabine dosing—time for a change? *Nat Rev Clin Oncol* **8**, 439-444 (2011).

41. Weiss JT*, et al.* Development and bioorthogonal activation of palladium-labile prodrugs of gemcitabine. *J Med Chem* **57**, 5395-5404 (2014).

42. Yarmolinsky MB, Haba GLDL. Inhibition by puromycin of amino acid incorporation into protein. *Proc Natl Acad Sci U S A* **45**, 1721-1729 (1959).

43. Xi J, Liu Y, Zhang L, Zhang B, Zhao J, Fang J. Redox dyshomeostasis-driven prodrug strategy for enhancing camptothecin-based chemotherapy: Selenization of SN38 as a case study. *Bioorg Chem* **160**, 108468 (2025).

44. Staben LR*, et al.* Targeted drug delivery through the traceless release of tertiary and heteroaryl amines from antibody-drug conjugates. *Nat Chem* **8**, 1112-1119 (2016).

45. Alouane A, Labruere R, Le Saux T, Schmidt F, Jullien L. Self-immolative spacers: kinetic aspects, structure-property relationships, and applications. *Angew Chem, Int Ed* **54**, 7492-7509 (2015).

46. Wang X, Zhuang Y, Wang Y, Jiang M, Yao L. The recent developments of camptothecin and its derivatives as potential anti-tumor agents. *Eur J Med Chem* **260**, 115710 (2023).

47. Bhuniya S*, et al.* An activatable theranostic for targeted cancer therapy and imaging. *Angew Chem, Int Ed* **53**, 4469-4474 (2014).

48. Kim EJ*, et al.* An activatable prodrug for the treatment of metastatic tumors. *J Am Chem Soc* **136**, 13888-13894 (2014).

49. Zhao L*, et al.* Baylis-Hillman adducts as a versatile module for constructing fuorogenic release system. *J Med Chem* **65**, 6056-6069 (2022).

50. Qin G*, et al.* A selective mitochondria-targeted fluorescent probe for imaging cysteine in drug-induced liver injury. *Talanta* **282**, 127056 (2024).

51. Qin G*, et al.* A nonconsumptive fluorescent probe for precise detection of hydrogen peroxide in nonalcoholic fatty liver disease and inflammation. *Anal Chem* **97**, 7195-7202 (2025).

52. Zhou Z, Lü, X., Zhu, L., Zhou, J., Huang, H., Zhang, C., Liu, X. . Construction of a stable TrxR1 knockout HCT-116 cell line using CRISPR/Cas9 gene editing system. *Chin J Biotechnol* **38**, 1074-1085 (2022).

53. Du Y, Zhang H, Lu J, Holmgren A. Glutathione and glutaredoxin act as a backup of human thioredoxin reductase 1 to reduce thioredoxin 1 preventing cell death by aurothioglucose*. *J Biol Chem* **287**, 38210-38219 (2012).

54. Mandal PK*, et al.* Loss of thioredoxin reductase 1 renders tumors highly susceptible to pharmacologic glutathione deprivation. *Cancer Res* **70**, 9505-9514 (2010).

55. Ma T*, et al.* Diselenides as novel effective fluorescence quenchers to construct a two-photon fluorescent probe for thiols in a mouse stroke model. *Chem Commun* **61**, 1910-1913 (2025).

56. Stafford WC*, et al.* Irreversible inhibition of cytosolic thioredoxin reductase 1 as a mechanistic basis for anticancer therapy. *Science Translational Medicine* **10**, eaaf7444 (2018).

57. Xue Y*, et al.* Stimulus-cleavable chemistry in the field of controlled drug delivery. *Chem Soc Rev* **50**, 4872-4931 (2021).

58. Deng Z, Hu J, Liu S. Disulfide-based self-Immolative linkers and functional bioconjugates for biological applications. *Macromol Rapid Comm* **41**, e1900531 (2020).

59. Zhang P, Wu J, Xiao F, Zhao D, Luan Y. Disulfide bond based polymeric drug carriers for cancer chemotherapy and relevant redox environments in mammals. *Med Res Rev* **38**, 1485-1510 (2018).

60. Zhao J, Li X, Ma T, Chang B, Zhang B, Fang J. Glutathione-triggered prodrugs: design strategies, potential applications, and perspectives. *Med Res Rev* **44**, 1013-1054 (2023).

61. Zhang C*, et al.* Design and synthesis of a ratiometric photoacoustic imaging probe activated by selenol for visual monitoring of pathological progression of autoimmune hepatitis. *Chem Sci* **12**, 4883-4888 (2021).

62. Moser P*, et al.* Fast release of carboxylic acid inside cells. *ChemMedChem*, e202500056 (2025).

63. Wang Q, Guan J, Wan J, Li Z. Disulfide based prodrugs for cancer therapy. *RSC Advances* **10**, 24397-24409 (2020).

64. Turell L, Botti H, Carballal S, Radi R, Alvarez B. Sulfenic acid—A key intermediate in albumin thiol oxidation. *J Chromatogr B* **877**, 3384-3392 (2009).

65. Jia H*, et al.* Fluorophore-dependent cleavage of disulfide bond leading to a highly selective fluorescent probe of thioredoxin. *Anal Chem* **91**, 8524-8531 (2019).

66. Lee MH*, et al.* Toward a chemical marker for inflammatory disease: A fluorescent probe for membrane-localized thioredoxin. *J Am Chem Soc* **136**, 8430-8437 (2014).

67. Wang Y, Zhang L, Chen L. Glutathione peroxidase-activatable two-photon ratiometric fluorescent probe for redox mechanism research in aging and mercury exposure mice models. *Anal Chem* **92**, 1997-2004 (2020).

68. Zuo X*, et al.* A fluorescent probe for specifically measuring the overall thioredoxin and glutaredoxin reducing activity in bacterial cells. *Analyst* **147**, 834-840 (2022).

69. Zhao Y, Zuo X, Liu S, Qian W, Tang X, Lu J. A Fluorescent Probe to Detect Quick Disulfide Reductase Activity in Bacteria. *Antioxidants* **11**, 377 (2022).

70. Lü X, Zhou, Z., Zhu, L., Zhou, J., Huang, H., Zhang, C., Liu, X. Construction and identification of a HEK293 cell line with stable TrxR1 overexpression. *J South Med Univ* **42**, 554-560 (2022).

71. Petukhova VZ*, et al.* Non-covalent inhibitors of thioredoxin glutathione reductase with schistosomicidal activity in vivo. *Nat Commun* **14**, 3737 (2023).

72. Zhong Z*, et al.* NFATc1-mediated expression of SLC7A11 drives sensitivity to TXNRD1 inhibitors in osteoclast

precursors. *Redox Biology* **63**, 102711 (2023).

73. Engelman R, Ziv T, Arnér ESJ, Benhar M. Inhibitory nitrosylation of mammalian thioredoxin reductase 1: Molecular characterization and evidence for its functional role in cellular nitroso-redox imbalance. *Free Radical Bio Med* **97**, 375-385 (2016).

74. Zhou J*, et al.* Discovery of novel hydroxyamidine based indoleamine 2,3-dioxygenase 1 (IDO1) and thioredoxin reductase 1 (TrxR1) dual inhibitors. *Eur J Med Chem* **245**, 114860 (2023).

75. Flowers B*, et al.* Pleiotropic anti-cancer activities of novel non-covalent thioredoxin reductase inhibitors against triple negative breast cancer. *Free Radical Bio Med* **227**, 201-209 (2025).

76. Fan Q-Z*, et al.* Design, synthesis, and biological evaluation of a novel indoleamine 2,3-dioxigenase 1 (IDO1) and thioredoxin reductase (TrxR) dual inhibitor. *Bioorg Chem* **105**, 104401 (2020).

77. Zhong M*, et al.* Synthesis and evaluation of Piperine analogs as thioredoxin reductase inhibitors to cause oxidative stress-induced cancer cell apoptosis. *Bioorg Chem* **138**, 106589 (2023).

78. Zheng Y-L*, et al.* Redox-based strategy for selectively inducing energy crisis inside cancer cells: an example of modifying dietary curcumin to target mitochondria. *J Agr Food Chem* **70**, 2898-2910 (2022).

79. Wang J*, et al.* Targeting thioredoxin reductase 1 by Andrographolide contributes to inducing ROS-mediated apoptosis in human NSCLC cells. *Chem-Biol Interact* **421**, 111778 (2025).

80. Wang R*, et al.* Pretargeted mitochondrial delivery of organoarsenicals for cancer immunotherapy. *J Am Chem Soc* **147**, 38534-38548 (2025).

81. Rullo A*, et al.* Unravelling the anti-cancer mechanisms elicited by non-covalent thioredoxin reductase inhibitors for triple negative breast cancer therapy. *Redox Biology*, 103980 (2025).

82. Zhong Z*, et al.* Beyond thiol-enzyme inhibition: sterically bulky NHC-Au(I) complexes are catalytically active anticancer agents with reprogrammed immunomodulatory function. *J Am Chem Soc*, doi: 10.1021/jacs.5c19777 (2026).

83. Zhang L, Zhao J, Yi M, Osama A, Fang J. Structural Optimization of Dithiaarsanes-Enhanced Cytotoxicity to Leukemia Cells With Improved Thioredoxin Reductase Inhibition. *Chem Asian J* **21**, e00977 (2026).

84. Seim GL, John SV, Arp NL, Fang Z, Pagliarini DJ, Fan J. Nitric oxide-driven modifications of lipoic arm inhibit α-ketoacid dehydrogenases. *Nat Chem Biol* **19**, 265-274 (2022).

85. Gu F*, et al.* Tumour microenvironment-responsive lipoic acid nanoparticles for targeted delivery of docetaxel to lung cancer. *Sci Rep* **6**, 36281 (2016).

86. Lv S-y*, et al.* Review of lipoic acid: from a clinical therapeutic agent to various emerging biomaterials. *Int J Pharm* **627**, 122201 (2022).

87. Kang DH, Kim J, Lee J, Kang SW. The small molecule peroxiredoxin mimetics restore growth factor signalings and reverse vascular remodeling. *Free Radical Bio Med* **229**, 300-311 (2025).

88. Kang DH*, et al.* Vascular injury involves the overoxidation of peroxiredoxin type II and is recovered by the peroxiredoxin activity mimetic that induces reendothelialization. *Circulation* **128**, 834-844 (2013).

89. Zeisel L*, et al.* Piperazine-fused cyclic disulfides unlock high-performance bioreductive probes of thioredoxins

and bifunctional reagents for thiol redox biology. *J Am Chem Soc* **146**, 5204-5214 (2024).

90. Felber JG*, et al.* Selective, modular probes for thioredoxins enabled by rational tuning of a unique disulfide structure motif. *J Am Chem Soc* **143**, 8791-8803 (2021).

91. Eberhardt J, Santos-Martins D, Tillack AF, Forli SJJoci, modeling. AutoDock Vina 1.2. 0: new docking methods, expanded force field, and python bindings. *J Chem Inf Model* **61**, 3891-3898 (2021).

92. Trott O, Olson AJJJocc. AutoDock Vina: improving the speed and accuracy of docking with a new scoring function, efficient optimization, and multithreading. *J Comput Chem* **31**, 455-461 (2010).

7. Acknowledgments

This research was supported by the China Postdoctoral Science Foundation under Grant Number 2025M783554 (J.Z.).

8. Author contributions

J.Z. conceived and led the study, designed and coordinated the overall experimental strategy, synthesized all compounds, performed all spectroscopic and HPLC analyses, processed and interpreted the data, wrote the original draft of the manuscript, and contributed funding support for the research. H.L. performed the TrxR1-knockout–related cellular imaging, cytotoxicity assays, and associated experiments (Fig. 7D, Fig. 9, and Supplementary Figs. 11, 16, 17 and 18). T.L. conducted the computational docking studies (Supplementary Figs. 6 and 12). J.W. conducted the cytotoxicity assays shown in Supplementary Fig. 9. B.C. provided prodrug Se1-DOX, and T.M. provided probe AFC-SS. M.Y. performed the cellular imaging experiments in Supplementary Fig. 15. S.-H.W. contributed computational docking support. X.L. analyzed the data and contributed to discussion. B.Z. provided instrumentation support and reviewed key data. C.Z. provided the HCT116 cell lines (WT, NC, and *TrxR1*-KO) and TrxR, and supervised the experimental design, execution, and data analysis of all HCT116-related studies, including the TRi-1 inhibition experiments. J.F. contributed to project conception, supervised the research, provided input on data interpretation and manuscript revision, and offered funding and instrumentation support. All authors reviewed and approved the final manuscript.

9. Competing interest

The authors declare no competing interests.

10. Figure Legends/Captions (for main text figures)

Fig. 1 Small-molecule chemical biology tools for selective TrxR targeting.

(A) Representative recognition motifs for TrxR activation. (B) TRFS probes reported previously. (C) TrxR-targeted prodrugs reported previously. (D) Proposed activation mechanism of TRFS-green. (E) Activation mechanism of Fast-TRFS.

Fig. 2 Structural determinants govern the reactivity of 1,2-dithiolane-based constructs. Cargo structure and linker configuration shape activation profiles in biological contexts.

Fig. 3 Synthesis of intermediates and target molecules.

(a) DCM, triphosgene, DMAP, 1,2-dithiolan-4-ol or cyclopentanol, rt; (b) DMF, TBSCl, DIPEA, rt; (c) DCM, triphosgene, DMAP, 1,2-dithiolan-4-ol, rt; (d) THF, TBAF, AcOH, rt; (e) DMF, TEA, rt; (f) DMF, TEA, rt; (g) DCM, DMAP, rt; (h) DMF, TEA, rt; (i) DMF, TBSCl, TEA, rt; (j) toluene, triphosgene, DMAP, 1,2-dithiolan-4-ol or 1,2-diselenolan-4-ol, 110 °C, then rt; (k) MeOH, HCl, rt; (l) DCM, TEA, 4-nitrophenyl chloroformate, rt; (m) DMF, DOX·HCl, TEA, rt; (n) toluene, triphosgene, DMAP, 1,2-dithiolan-4-ol, 110 °C, then rt; (o) DCM, triphosgene, TEA, 1,2-dithiolan-4-amine, rt; (p) DCM, TEA, rt.

Fig. 4 Reductive-responsive fluorescence changes of S-CPT, S1-SN38, and S2-SN38.

(A, B) Time-dependent fluorescence spectra of S-CPT upon addition of GSH or TrxR (λ_{ex} = 365 nm). (C, D) Time-dependent fluorescence spectra of S1-SN38 upon addition of GSH or TrxR (λ_{ex} = 380 nm). (E, F) Time-dependent fluorescence spectra of S2-SN38 upon addition of GSH or TrxR (λ_{ex} = 380 nm). (G) Proposed activation mechanism of S-CPT. All prodrugs were tested at a concentration of 10 μM. Reaction conditions: GSH (1 mM), TrxR (50 nM), and NADPH (200 μM) to support TrxR catalysis. All assays were conducted at 37 °C. Source data are provided as a Source Data file.

Fig. 5 Reductive responsiveness of S-CPT, S1-SN38, S2-SN38, S1-Gem, and S-PTX.

(A–D) Percentage of drug release from S-CPT (10 μM), S1-SN38 (10 μM), S2-SN38 (10 μM), S1-Gem (50 μM), and S-PTX (20 μM) in response to GSH or TrxR. (E–H) Percentage of residual prodrug under the same conditions. Reaction conditions: GSH (1 mM), TrxR (50 nM), and NADPH (200 μM) to support TrxR catalysis; all reactions conducted at 37 °C. The original chromatograms are provided in Supplementary Fig. 3. Source data are provided as a Source Data

file.

Fig. 6 Redox-responsive fluorescence changes of S1-DOX, S2-DOX, Se1-DOX, and Se2-DOX. (A–C) Time-dependent fluorescence spectra of S1-DOX upon incubation with DTT, TrxR, or GSH, respectively. (D–F) Time-dependent fluorescence spectra of S2-DOX in response to DTT, TrxR, or GSH, respectively. (G–I) Time-dependent fluorescence spectra of Se1-DOX upon exposure to DTT, TrxR, or GSH, respectively. (J–L) Time-dependent fluorescence spectra of Se2-DOX following treatment with DTT, TrxR, or GSH, respectively. The excitation/emission wavelengths for all prodrugs were set at 480/590 nm. Prodrug concentration: 10 μM. Assay conditions: DTT (1 mM), GSH (5 mM), TrxR (50 nM), and NADPH (200 μM) for TrxR catalysis. All experiments were conducted at 37 °C. Source data are provided as a Source Data file.

Fig. 7 Activation of S1-DOX mediated by TrxR.

(A) Time-dependent fluorescence enhancement of S1-DOX upon incubation with different TrxR concentrations (10 nM, 25 nM, and 50 nM). (B) Fluorescence selectivity of S1-DOX in the presence of various biological species (24 h). (C) Quantitative analysis of DOX release from S1-DOX induced by different biological species (24 h). (D) Comparison of S1-DOX cytotoxicity in HCT116, HCT116-NC, and HCT-*TrxR1*-KO cells (24 h). Cells treated with an equal volume of DMSO served as the vehicle control. Data are presented as mean ± SD (n = 3 per group). All replicates represent independent biological replicates. Source data are provided as a Source Data file.

Fig. 8 Activation of probes S-Cou and S1-Cou by variours reducing agents.

(A) Fluorescence activation of S-Cou follows the same carbamate cleavage mechanism as previously reported TRFS probes. (B–D) Time-dependent fluorescence emission spectra of S-Cou upon incubation with DTT, TrxR, and GSH, respectively. (E) Disulfide bond cleavage drives fluorescence activation of S1-Cou, following a mechanism analogous to the urea-linked probe Fast-TRFS. (F–H) Time-dependent fluorescence emission spectra of S1-Cou in response to DTT,

TrxR, and GSH, respectively. In (G), the yellow line represents S1-Cou incubated with NADPH for 60 minutes, while the red line depicts S1-Cou co-incubated with TrxR and NADPH under identical conditions. Excitation/emission wavelengths were 370/490 nm for S-Cou and 330/432 nm for S1-Cou. All probes were tested at a concentration of 10 μM. The assay conditions included DTT (1 mM), GSH (5 mM), and TrxR (50 nM), with NADPH (200 μM) required for TrxR activity. All incubations were conducted at 37 °C. Source data are provided as a Source Data file.

Fig. 9 Cellular imaging of TrxR activity using S-Cou and TRFS-green.
(A) Fluorescence imaging of S-Cou in HCT116, HCT116-NC, and HCT116-*TrxR1*-KO cells. (B) Quantification of S-Cou fluorescence intensity in the same cell lines by flow cytometry. (C) Fluorescence imaging of TRFS-green in HCT116, HCT116-NC, and HCT116-*TrxR1*-KO cells. (D) Flow cytometric quantification of TRFS-green fluorescence intensity. (E) TrxR1 inhibition in HCT116 cells by TRi-1, followed by fluorescence imaging with TRFS-green. (F) Flow cytometric quantification of TRFS-green fluorescence in HCT116 cells treated with auranofin (AF) as a positive control for TrxR inhibition. The experimental concentration of S-Cou and TRFS-green was 10 μM. Scale bars, 25 μm (A) and 75 μm (C, E). Data are presented as mean ± SD from three independent biological replicates. Statistical analyses in (B), (D) and (F) were performed using one-way ANOVA. Source data are provided as a Source Data file.

Fig. 10 Mechanistic insights into TrxR- and GSH-mediated cargo release.
(A) Schematic illustration of the selective activation and cargo release by TrxR in amine-containing molecules, while monothiols (e.g., GSH) fail to induce activation under the same conditions. (B) Hydroxyl-functionalized cargo enables efficient activation by GSH. (C) The 1,2-dithiolane-4-ol scaffold provides a versatile platform for designing redox-responsive molecules with distinct activation mechanisms. Pathway 1 enables TrxR-dependent activation of 1,2-dithiolane derivatives, yet selectivity is strictly governed by molecular architecture. Pathway 2 demonstrates pan-thiol reactivity, with both LMW and protein thiols mediating activation independent of TrxR specificity.

Editor Summary:
The cyclic five-membered disulfide 1,2-dithiolane holds promise as a recognition unit in probe design and drug development, but potential limitations in activation specificity, such as the diminished selectivity toward thioredoxin reductase (TrxR), raise concerns about its reliability in biological settings. Here, the authors systematically evaluate the activation behaviour of 1,2-dithiolane by synthesizing a panel of prodrugs and fluorescent probes incorporating either amine- or hydroxyl-linked cargoes, and show that TrxR-mediated selective activation of the 1,2-dithiolane unit is achievable when the cargo is incorporated within an amine-based framework.

Peer Review Information:
Nature Communications thanks Lin Yuan and the other anonymous reviewers for their contribution to the peer review of this work. [A peer review file is available.]

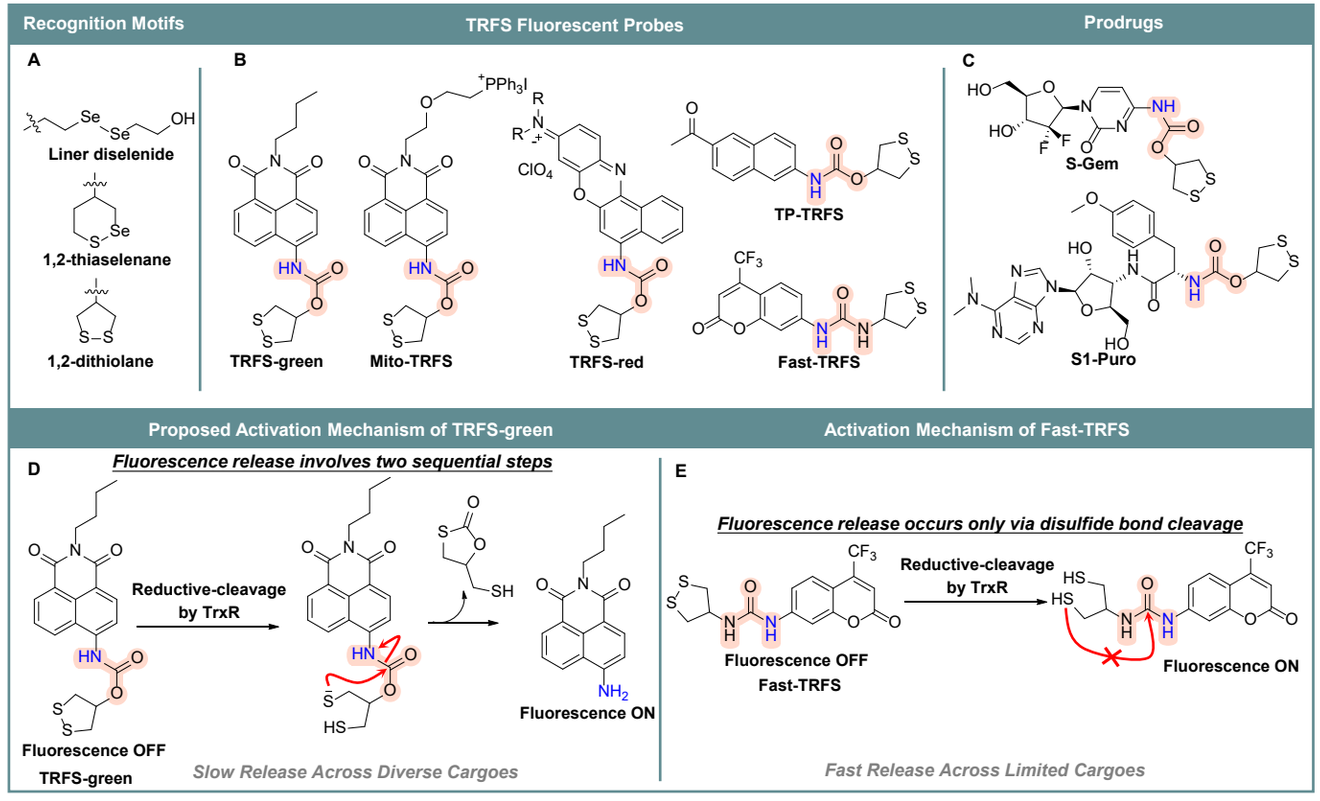
Recognition Motifs
TRFS Fluorescent Probes
Prodrugs
A
B
C
Liner diselenide
1,2-thiaselenane
1,2-dithiolane
TRFS-green
Mito-TRFS
TRFS-red
TP-TRFS
Fast-TRFS
S-Gem
S1-Puro
Proposed Activation Mechanism of TRFS-green
Activation Mechanism of Fast-TRFS
D
Fluorescence release involves two sequential steps
Reductive-cleavage by TrxR
Fluorescence OFF
TRFS-green
Fluorescence ON
Slow Release Across Diverse Cargoes
E
Fluorescence release occurs only via disulfide bond cleavage
Reductive-cleavage by TrxR
Fluorescence OFF
Fast-TRFS
Fluorescence ON
Fast Release Across Limited Cargoes

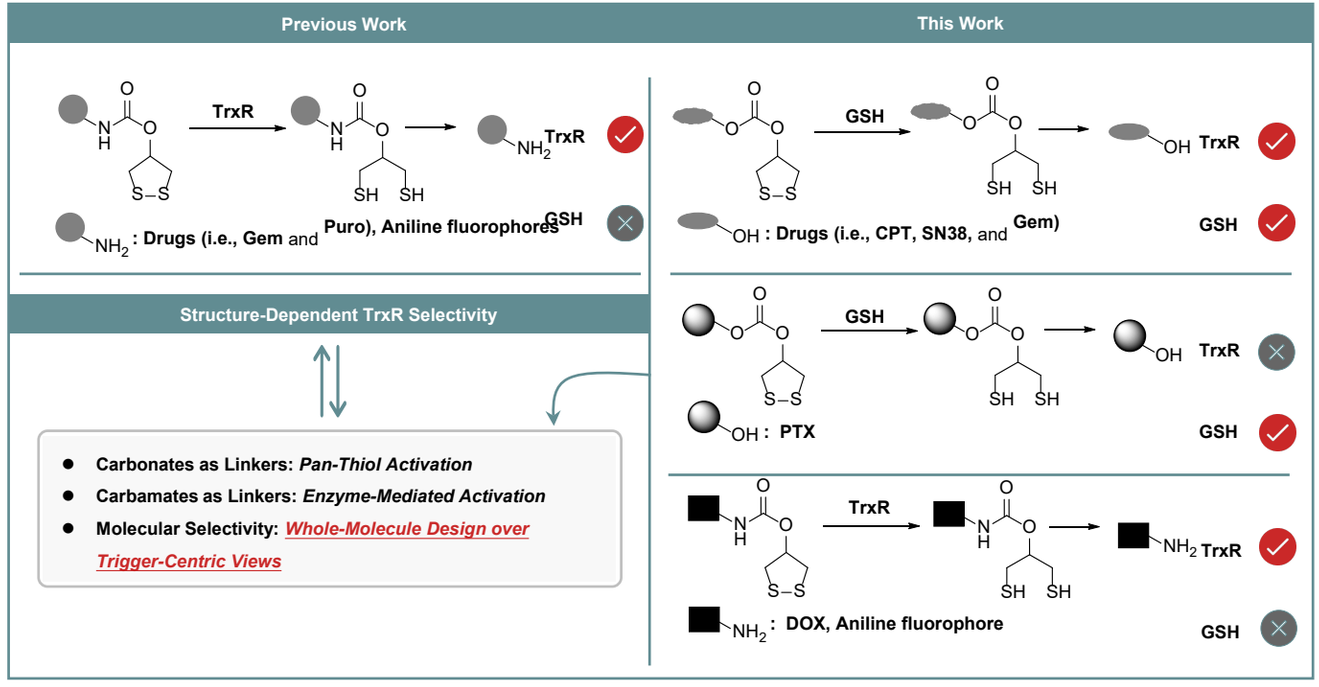
Previous Work
This Work
TrxR
GSH
: Drugs (i.e., Gem and Puro), Aniline fluorophores
: Drugs (i.e., CPT, SN38, and Gem)
: PTX
: DOX, Aniline fluorophore
Structure-Dependent TrxR Selectivity
Carbonates as Linkers: Pan-Thiol Activation
Carbamates as Linkers: Enzyme-Mediated Activation
Molecular Selectivity: Whole-Molecule Design over Trigger-Centric Views

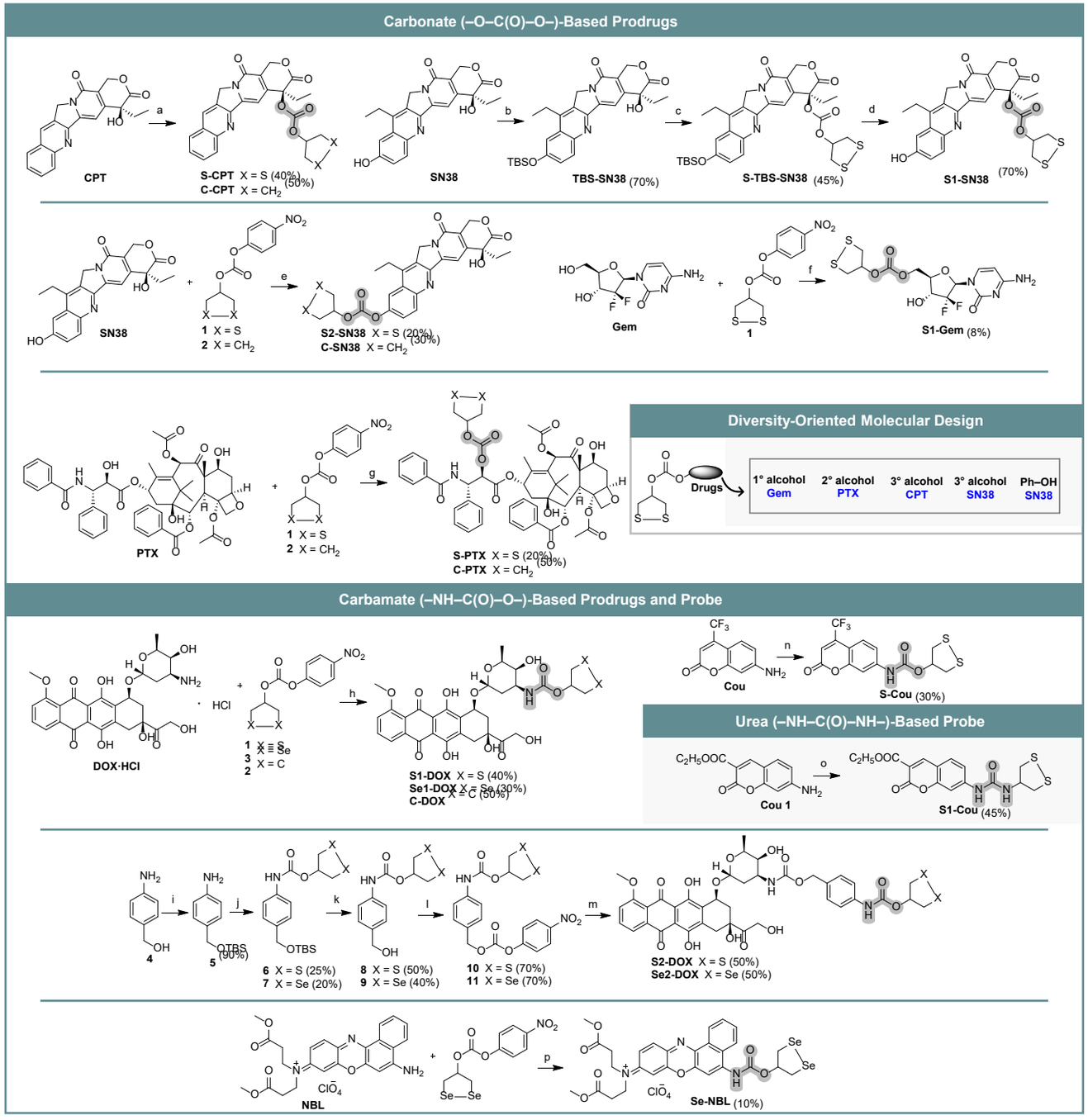
Carbonate (–O–C(O)–O–)-Based Prodrugs
CPT
S-CPT X = S (40%)
C-CPT X = CH2 (50%)
SN38
TBS-SN38 (70%)
S-TBS-SN38 (45%)
S1-SN38 (70%)
SN38
1 X = S
2 X = CH2
S2-SN38 X = S (20%)
C-SN38 X = CH2 (30%)
Gem
1
S1-Gem (8%)
PTX
1 X = S
2 X = CH2
S-PTX X = S (20%)
C-PTX X = CH2 (50%)
Diversity-Oriented Molecular Design
Drugs
1° alcohol Gem
2° alcohol PTX
3° alcohol CPT
3° alcohol SN38
Ph–OH SN38
Carbamate (–NH–C(O)–O–)-Based Prodrugs and Probe
DOX·HCl
1 X = S
3 X = Se
2 X = C
S1-DOX X = S (40%)
Se1-DOX X = Se (30%)
C-DOX X = C (50%)
Cou
S-Cou (30%)
Urea (–NH–C(O)–NH–)-Based Probe
Cou 1
S1-Cou (45%)
4
5 (90%)
6 X = S (25%)
7 X = Se (20%)
8 X = S (50%)
9 X = Se (40%)
10 X = S (70%)
11 X = Se (70%)
S2-DOX X = S (50%)
Se2-DOX X = Se (50%)
NBL
Se-NBL (10%)

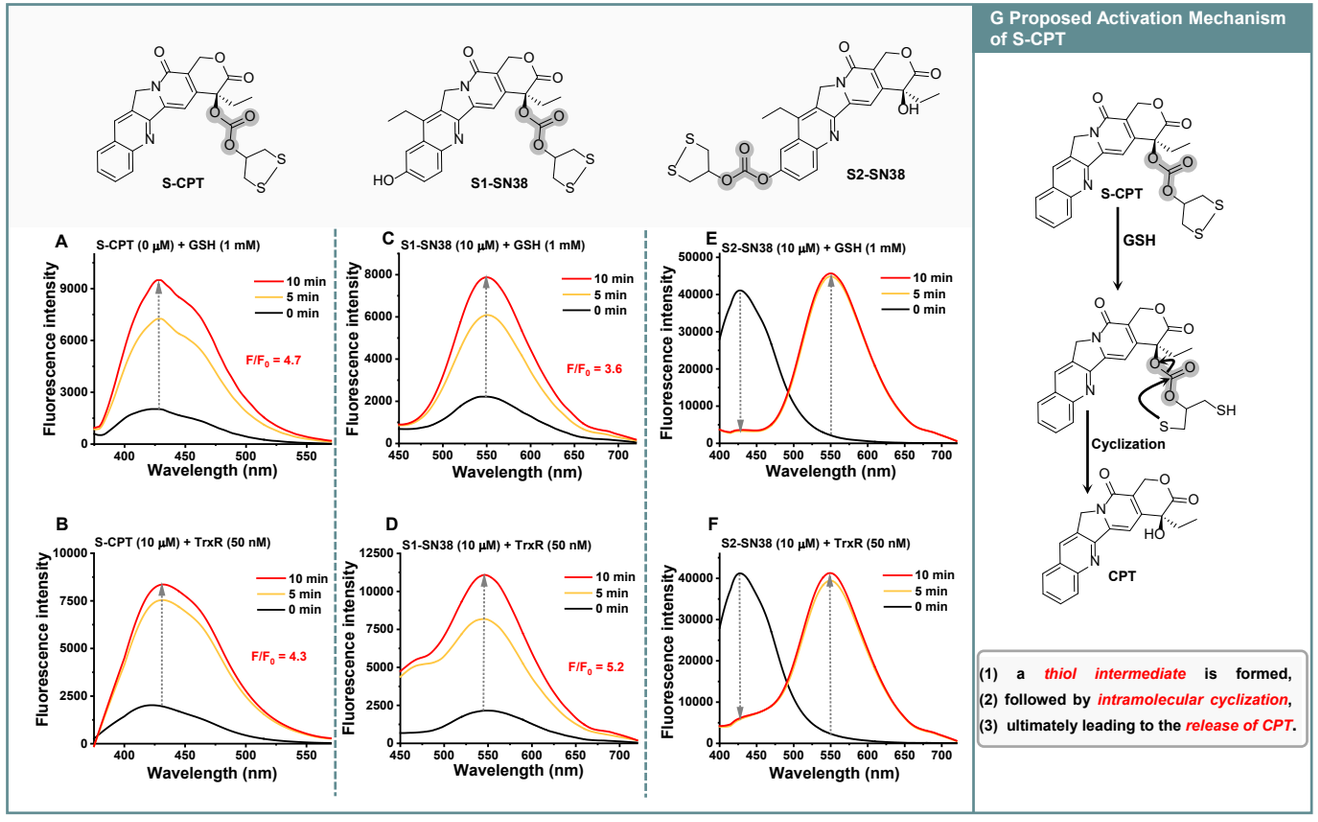
S-CPT
S1-SN38
S2-SN38
A
S-CPT (0 μM) + GSH (1 mM)
B
S-CPT (10 μM) + TrxR (50 nM)
C
S1-SN38 (10 μM) + GSH (1 mM)
D
S1-SN38 (10 μM) + TrxR (50 nM)
E
S2-SN38 (10 μM) + GSH (1 mM)
F
S2-SN38 (10 μM) + TrxR (50 nM)
10 min
5 min
0 min
F/F0 = 4.7
F/F0 = 4.3
F/F0 = 3.6
F/F0 = 5.2
Fluorescence intensity
Wavelength (nm)
G Proposed Activation Mechanism of S-CPT
GSH
Cyclization
CPT
(1) a thiol intermediate is formed,
(2) followed by intramolecular cyclization,
(3) ultimately leading to the release of CPT.

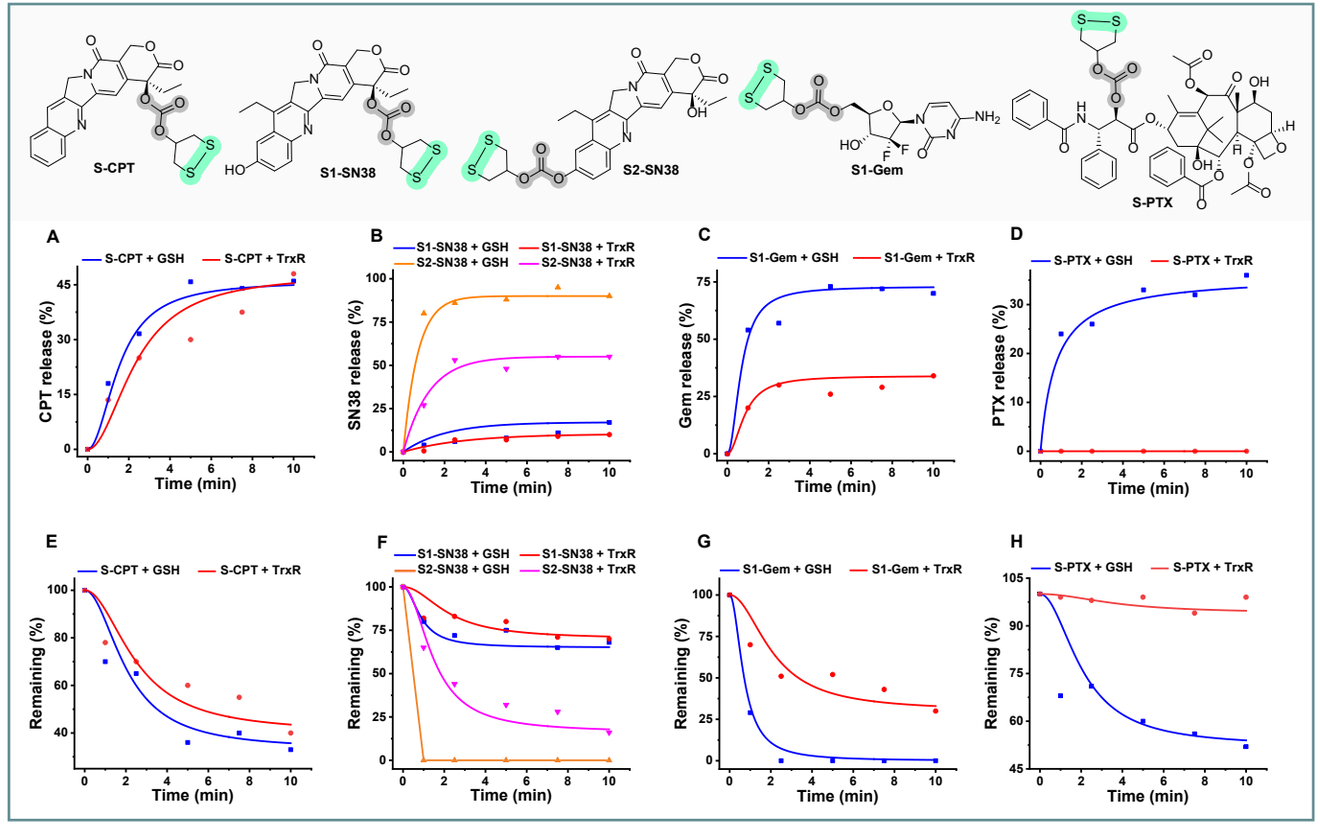
S-CPT
S1-SN38
S2-SN38
S1-Gem
S-PTX
A
S-CPT + GSH
S-CPT + TrxR
CPT release (%)
Time (min)
B
S1-SN38 + GSH
S1-SN38 + TrxR
S2-SN38 + GSH
S2-SN38 + TrxR
SN38 release (%)
Time (min)
C
S1-Gem + GSH
S1-Gem + TrxR
Gem release (%)
Time (min)
D
S-PTX + GSH
S-PTX + TrxR
PTX release (%)
Time (min)
E
S-CPT + GSH
S-CPT + TrxR
Remaining (%)
Time (min)
F
S1-SN38 + GSH
S1-SN38 + TrxR
S2-SN38 + GSH
S2-SN38 + TrxR
Remaining (%)
Time (min)
G
S1-Gem + GSH
S1-Gem + TrxR
Remaining (%)
Time (min)
H
S-PTX + GSH
S-PTX + TrxR
Remaining (%)
Time (min)

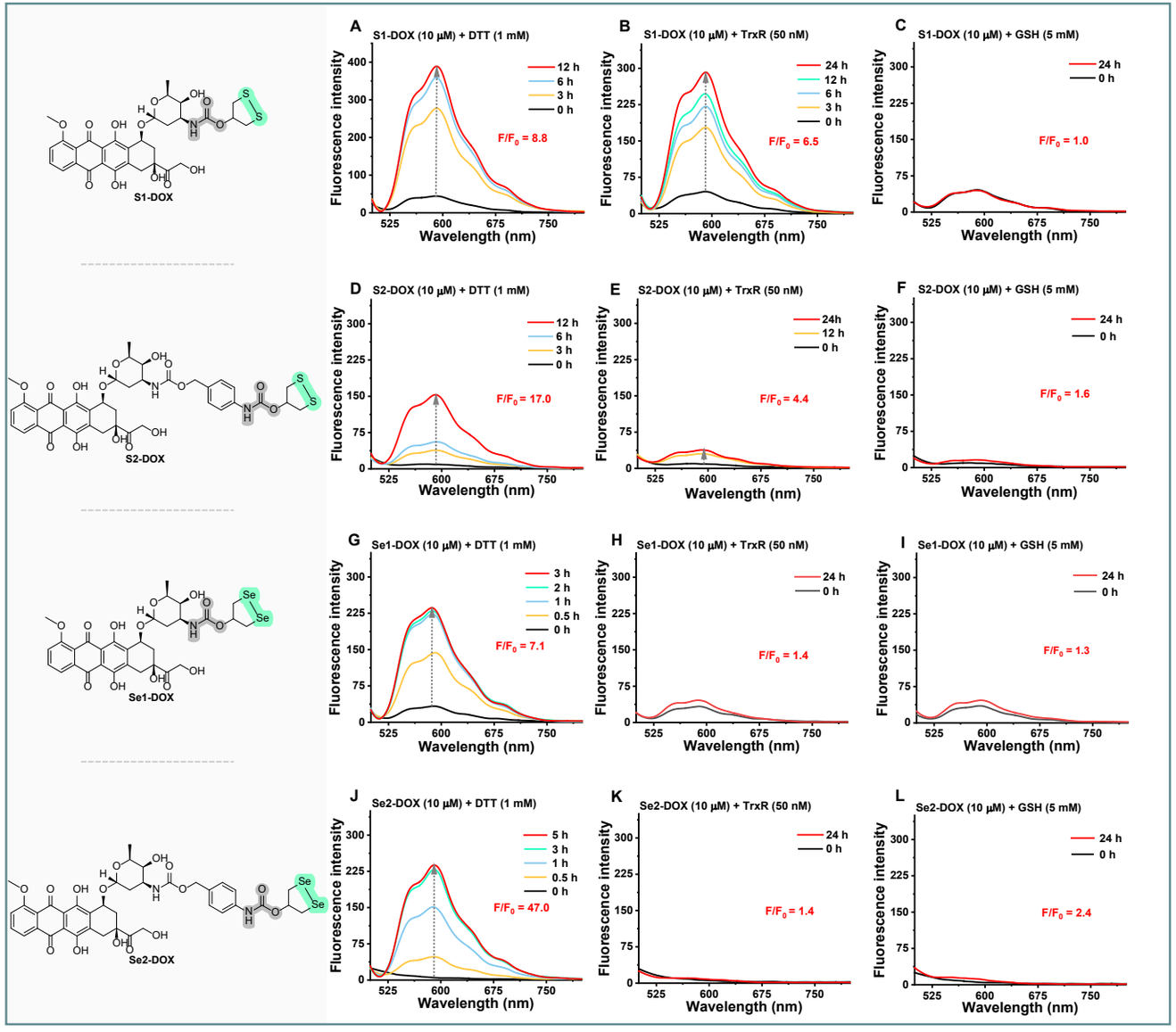
S1-DOX
S2-DOX
Se1-DOX
Se2-DOX
A
S1-DOX (10 μM) + DTT (1 mM)
12 h
6 h
3 h
0 h
F/F0 = 8.8
B
S1-DOX (10 μM) + TrxR (50 nM)
24 h
12 h
6 h
3 h
0 h
F/F0 = 6.5
C
S1-DOX (10 μM) + GSH (5 mM)
24 h
0 h
F/F0 = 1.0
D
S2-DOX (10 μM) + DTT (1 mM)
12 h
6 h
3 h
0 h
F/F0 = 17.0
E
S2-DOX (10 μM) + TrxR (50 nM)
24h
12 h
0 h
F/F0 = 4.4
F
S2-DOX (10 μM) + GSH (5 mM)
24 h
0 h
F/F0 = 1.6
G
Se1-DOX (10 μM) + DTT (1 mM)
3 h
2 h
1 h
0.5 h
0 h
F/F0 = 7.1
H
Se1-DOX (10 μM) + TrxR (50 nM)
24 h
0 h
F/F0 = 1.4
I
Se1-DOX (10 μM) + GSH (5 mM)
24 h
0 h
F/F0 = 1.3
J
Se2-DOX (10 μM) + DTT (1 mM)
5 h
3 h
1 h
0.5 h
0 h
F/F0 = 47.0
K
Se2-DOX (10 μM) + TrxR (50 nM)
24 h
0 h
F/F0 = 1.4
L
Se2-DOX (10 μM) + GSH (5 mM)
24 h
0 h
F/F0 = 2.4
Fluorescence intensity
Wavelength (nm)

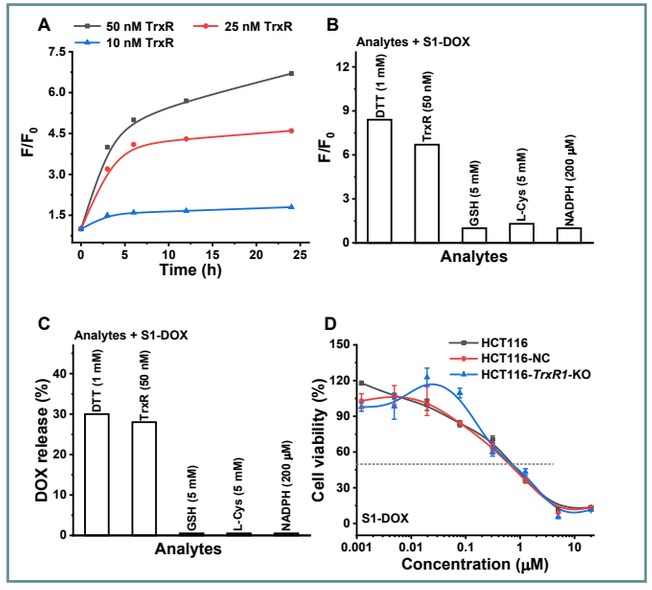
A
50 nM TrxR
25 nM TrxR
10 nM TrxR
F/F0
Time (h)
B
Analytes + S1-DOX
DTT (1 mM)
TrxR (50 nM)
GSH (5 mM)
L-Cys (5 mM)
NADPH (200 μM)
F/F0
Analytes
C
Analytes + S1-DOX
DOX release (%)
Analytes
D
HCT116
HCT116-NC
HCT116-TrxR1-KO
Cell viability (%)
S1-DOX
Concentration (μM)

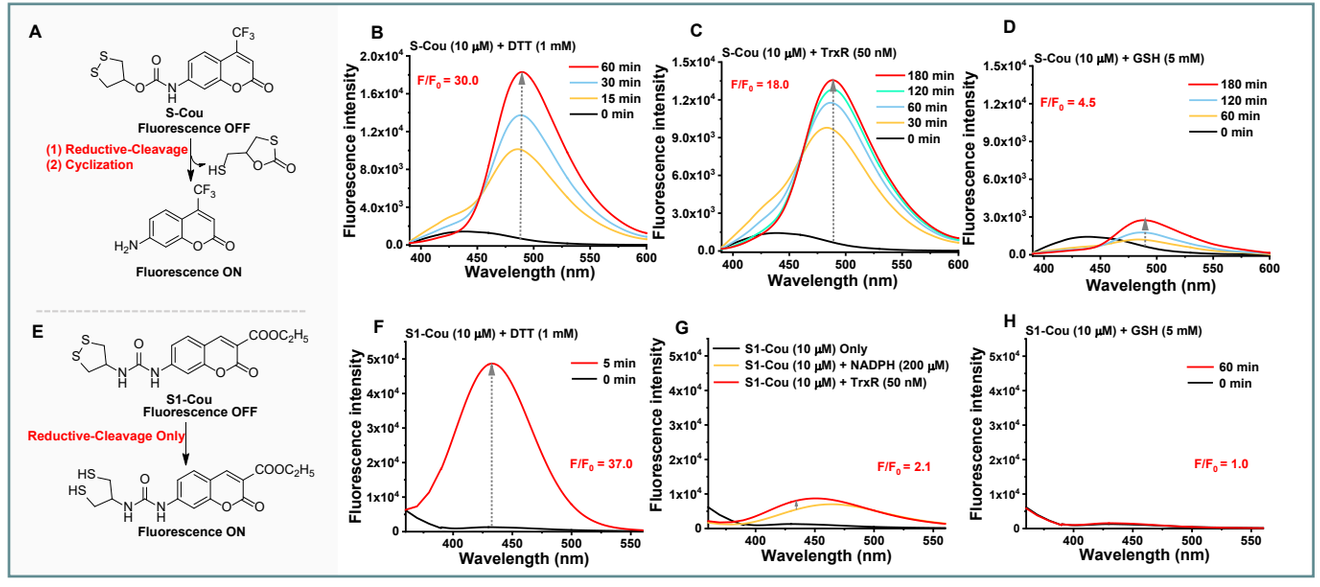
A
S-Cou
Fluorescence OFF
(1) Reductive-Cleavage
(2) Cyclization
Fluorescence ON
E
S1-Cou
Fluorescence OFF
Reductive-Cleavage Only
Fluorescence ON
B
S-Cou (10 μM) + DTT (1 mM)
F/F0 = 30.0
60 min
30 min
15 min
0 min
C
S-Cou (10 μM) + TrxR (50 nM)
F/F0 = 18.0
180 min
120 min
60 min
30 min
0 min
D
S-Cou (10 μM) + GSH (5 mM)
F/F0 = 4.5
180 min
120 min
60 min
0 min
F
S1-Cou (10 μM) + DTT (1 mM)
F/F0 = 37.0
5 min
0 min
G
S1-Cou (10 μM) Only
S1-Cou (10 μM) + NADPH (200 μM)
S1-Cou (10 μM) + TrxR (50 nM)
F/F0 = 2.1
H
S1-Cou (10 μM) + GSH (5 mM)
60 min
0 min
F/F0 = 1.0
Fluorescence intensity
Wavelength (nm)

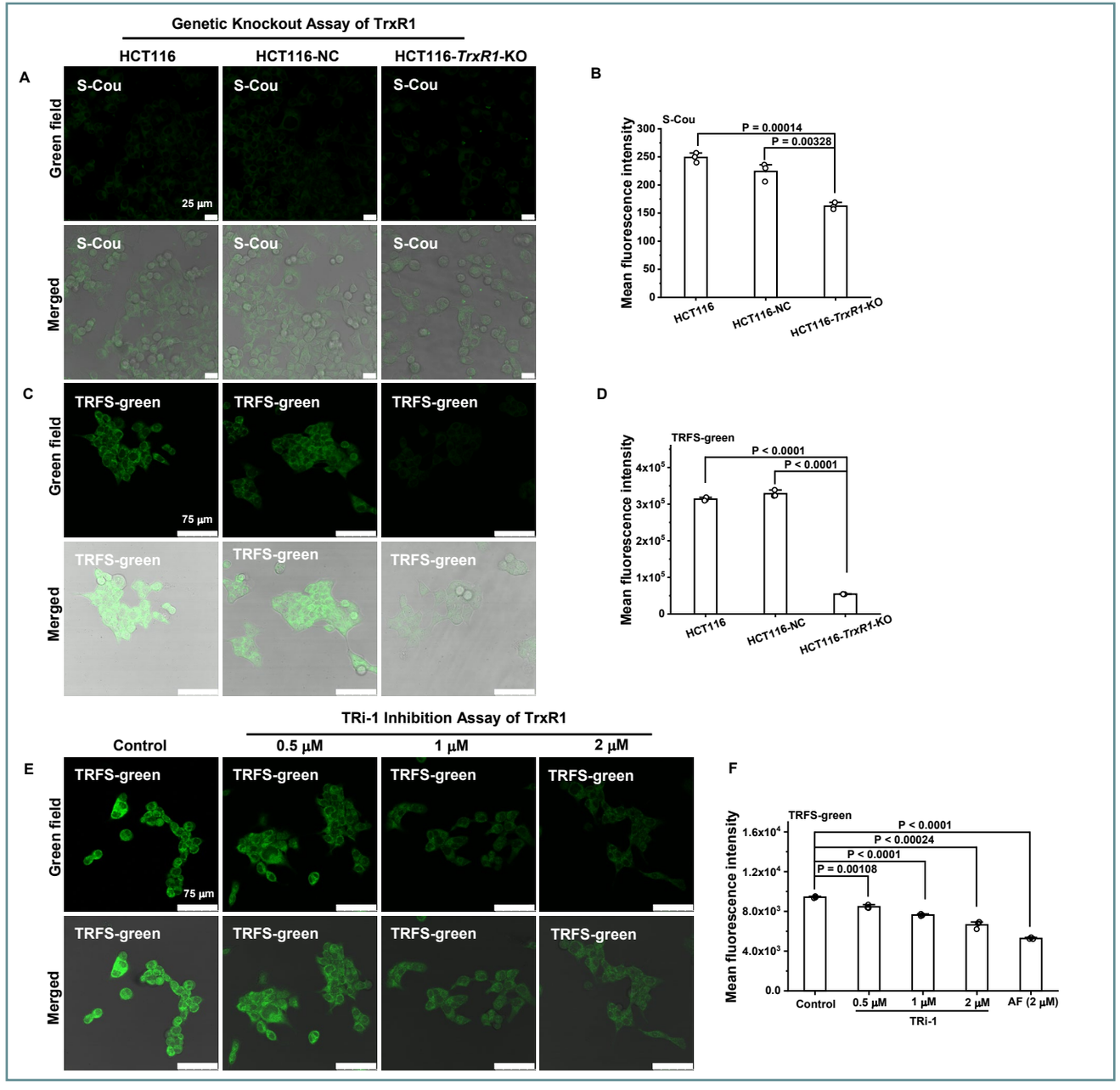
Genetic Knockout Assay of TrxR1
HCT116
HCT116-NC
HCT116-TrxR1-KO
A
Green field
Merged
S-Cou
25 μm
B
Mean fluorescence intensity
P = 0.00014
P = 0.00328
HCT116
HCT116-NC
HCT116-TrxR1-KO
C
TRFS-green
75 μm
D
P < 0.0001
P < 0.0001
TRi-1 Inhibition Assay of TrxR1
Control
0.5 μM
1 μM
2 μM
E
F
P < 0.0001
P < 0.00024
P < 0.0001
P = 0.00108
AF (2 μM)
TRi-1

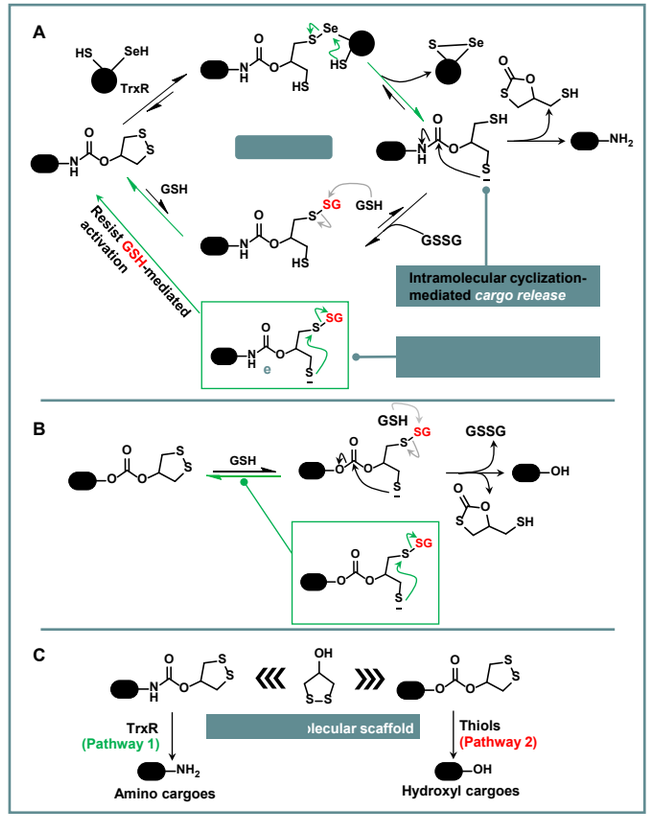
A
HS
SeH
TrxR
Se
S
Se
HS
HS
O
O
S
SH
NH2
GSH
SG
GSH
GSSG
Resist GSH-mediated activation
Intramolecular cyclization-mediated cargo release
e
B
GSH
GSH
SG
GSSG
OH
SH
C
OH
TrxR
(Pathway 1)
NH2
Amino cargoes
lecular scaffold
Thiols
(Pathway 2)
OH
Hydroxyl cargoes